Published in final edited form as:

Cell. 2016 September 22; 167(1): 233–247.e17. doi:10.1016/j.cell.2016.08.056.

Editing DNA methylation in the mammalian genome

X Shawn Liu[1,5], **Hao Wu**[1,5], **Xiong Ji**[1,3], **Yonatan Stelzer**[1], **Xuebing Wu**[1], **Szymon Czauderna**[1,4], **Jian Shu**[1], **Daniel Dadon**[1,2], **Richard A. Young**[1,2], and **Rudolf Jaenisch**[1,2,6,7]

[1]Whitehead Institute for Biomedical Research, Cambridge, MA 02142, USA [2]Department of Biology, Massachusetts Institute of Technology, Cambridge, MA 02142, USA [4]Department of Medical Biotechnology, Faculty of Biochemistry, Biophysics, and Biotechnology, Jagiellonian University, Poland

SUMMARY

Mammalian DNA methylation is a critical epigenetic mechanism orchestrating gene expression networks in many biological processes. However, investigation of the functions of specific methylation events remains challenging. Here, we demonstrate that fusion of Tet1 or Dnmt3a with a catalytically inactive Cas9 (dCas9) enables targeted DNA methylation editing. Targeting of the dCas9-Tet1 or -Dnmt3a fusion protein to methylated or unmethylated promoter sequences caused activation or silencing, respectively, of an endogenous reporter. Targeted demethylation of the *BDNF* promoter IV or the *MyoD* distal enhancer by dCas9-Tet1 induced BDNF expression in post-mitotic neurons or activated MyoD facilitating reprogramming of fibroblasts into myoblasts, respectively. Targeted *de novo* methylation of a CTCF loop anchor site by dCas9-Dnmt3a blocked CTCF binding and interfered with DNA looping, causing altered gene expression in the neighboring loop. Finally, we show that these tools can edit DNA methylation in mice demonstrating their wide utility for functional studies of epigenetic regulation.

Graphical Abstract

[6,7]Correspondence should be addressed to Rudolf Jaenisch as the Lead Contact, jaenisch@wi.mit.edu, Phone: 617-258-5186.
[3]Present address: School of Life Sciences, Peking-Tsinghua Center for Life Sciences, Peking University, Beijing 100871, China
[5]These authors contributed equally to this work

Author Contributions

X.S.L. and R.J. conceived the idea for this project. X.S.L. and H.W. designed and conducted the experiments and interpreted the data. X.J. performed ChIP and 3C assay, Y.S. generated Snrpn-GFP reporter ES cell lines and IG-DMR$^{GFP/Pat}$ reporter mice. S.C., X.W. and J.S. assisted with sequencing analysis. X.S.L., H.W. and R.J. wrote the manuscript with inputs from all the other authors.

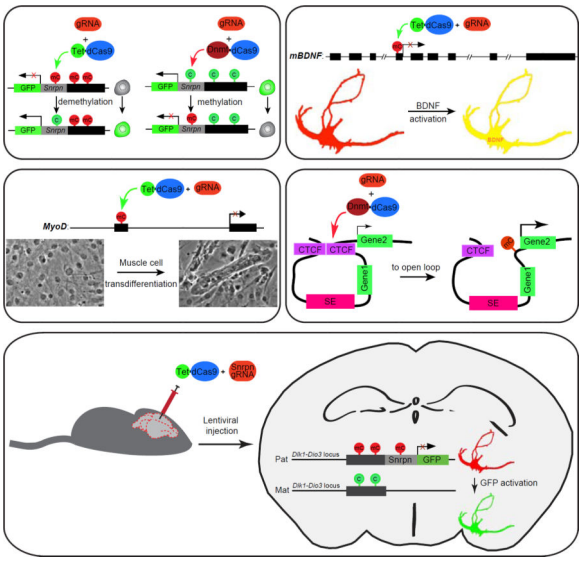

Introduction

Mammalian DNA methylation at 5-cytosine plays critical roles in many biological processes, including genomic imprinting, cell fate determination, chromatin architecture organization, and regulation of gene expression (Bird, 2002; Jaenisch and Bird, 2003; Smith and Meissner, 2013). Genetic studies have revealed that DNA methylation is essential for mammalian development and adaptation to environmental signals (Jaenisch and Bird, 2003). Abnormal DNA methylation has been observed in cancer and neurological disorders (Robertson, 2005). Owing to the advancement in sequencing technologies, single-nucleotide resolution methylation maps for many types of human and mouse cells and tissues have been depicted (Lister et al., 2013; Lister et al., 2009). Importantly, these maps have allowed for the identification of differentially methylated regions (DMRs) at base pair resolution during different stages of normal development as well as disease (De Jager et al., 2014; Landau et al., 2014). However, investigation of the functional significance of these DMRs remains a challenge due to lack of appropriate molecular tools that enable efficient editing of DNA methylation in a targeted manner.

We set out to establish such a toolbox by hybridization of the key enzymes in DNA methylation pathway with reprogrammable sequence-specific DNA-targeting molecular machinery. DNA methylation is established by two *de novo* DNA methyltransferases (Dnmt3a/b), and is maintained by Dnmt1 (Smith and Meissner, 2013). Gene activation during development is associated with demethylation of promoter and enhancer sequences with the best-understood mechanism being passive demethylation by inhibition of Dnmt1. In addition, demethylation can be achieved through oxidation of the methyl group by TET (ten-eleven translocation) dioxygenases to form 5-hydroxymethylcytosine (5-hmC), and then restoration into unmodified cytosines by either DNA replication-dependent dilution or DNA glycosylase-initiated base excision repair (BER), a process termed as active demethylation and proposed to operate during specific developmental stages such as preimplantation embryos or in post-mitotic neurons (Wu and Zhang, 2014).

Clustered regularly interspaced palindromic repeats (CRISPR), a type II bacterial adaptive immune system, has been modified to target the Cas9 nuclease to desired genomic loci with sequence-specific guide RNAs for genome editing (Cong et al., 2013; Jinek et al., 2012; Mali et al., 2013). Importantly, a catalytically inactive Cas9 (dCas9) was generated and engineered in several systems as a DNA targeting module to bring effector proteins such as transcriptional activator/suppressor, chromatin modifier, and green fluorescence protein to regulate gene expression, to modify chromatin, and to image genomic loci respectively (Chen et al., 2013; Gilbert et al., 2013; Hilton et al., 2015; Jinek et al., 2012; Konermann et al., 2015; Qi et al., 2013).

In this study, we demonstrate that fusion of dCas9 with the Tet1 enzymatic domain or Dnmt3a allows for targeted erasure or establishment of DNA methylation, respectively. As a proof of principle, we first induced alterations to DNA methylation in two synthetic methylation reporters integrated in mouse embryonic stem cells (mESCs). Our results show that targeted demethylation of *BDNF* promoter IV is sufficient to activate its expression in mouse cortical neurons, and that targeted demethylation of a *MyoD* distal enhancer promotes reprogramming of fibroblasts into myoblasts and facilitates myotube formation. With dCas9-Dnmt3a, we demonstrate that targeted methylation at CTCF binding sites is able to block CTCF recruitment and to alter the expression of genes in the neighborhood loop by increasing their interaction frequencies with the super-enhancers insulated in the targeted loops. Furthermore, lentiviral delivery of dCas9-Tet1 with target gRNAs into mice enabled *in vivo* activation of a methylation reporter by demethylation of its promoter. Thus, dCas9-Tet1 and dCas9-Dnmt3a provide powerful tools to investigate the functional significance of DNA methylation in a locus-specific manner.

RESULTS

A modified CRISPR system to edit DNA methylation

To achieve targeted editing of DNA methylation, we fused dCas9 with enzymes in the methylation/demethylation pathway (Fig 1A). Based on previous studies using the TALE system to target specific CpGs (Bernstein et al., 2015; Maeder et al., 2013), Tet1 and Dnmt3a were chosen as the effectors in our system. Co-expression of sequence-specific guide RNA (gRNA) would be expected to target dCas9-Tet1 or dCas9-Dnmt3a to the specific locus and mediate modification of DNA methylation status without altering the DNA sequence. To optimize this chimeric CRISPR/dCas9-effector system, we tested two types of dCas9-Tet1 lentiviral constructs with nuclear localization signal (NLS) at different positions: dCas9-NLS-Tet1 and NLS-dCas9-NLS-Tet1 (Fig S1A and S1B). We also tested two types of gRNA lentiviral constructs, a widely used chimeric single-guide RNA referred as gRNA (Jinek et al., 2012) and a modified guide RNA with enhanced capacity to guide Cas9 to the designed genomic locus referred as E-gRNA (Chen et al., 2013). Both gRNA constructs contain a *puro* selection cassette and a Cherry fluorescence protein cassette driven by an independent CMV promoter that allows for Fluorescence Activated Cell Sorting (FACS) of gRNA-expressing cells after lentiviral transduction (Fig S1A). Characterization of these constructs showed a robust gRNA-induced nuclear translocation for the dCas9-NLS-Tet1 construct (Fig S1C–E), and thus this construct was chosen for all experiments in

order to minimize non-specific modifications of DNA. Two types of gRNA behaved similarly (Fig S1C–E) and thus were used interchangeably.

dCas9-Tet1 and dCas9-Dnmt3a enable targeted alterations of CpG methylation state

To assess whether the dCas9-Tet1 and -Dnmt3a fusion constructs would induce demethylation or *de novo* methylation, respectively, of specific sequences, we utilized a methylation reporter system previously developed in our laboratory (Stelzer et al., 2015). This reporter system consists of a synthetic methylation-sensing promoter (conserved sequence elements from the promoter of an imprinted gene, *Snrpn*) that controls the expression of a green fluorescence protein (GFP). Insertion of this reporter construct into a genomic locus was shown to faithfully report on the methylation state of the adjacent sequences (Stelzer et al, 2015).

a. Demethylation of specific CpGs—To test whether defined sequences could be demethylated, we introduced the dCas9-Tet1 construct in combination with gRNAs to target the Snrpn-GFP reporter inserted into the *Dazl* promoter (Fig 1B and Fig S2A). *Dazl* is a germ cell specific gene, which is hypermethylated and not active in ES cells, and thus the GFP reporter is not expressed. To activate GFP expression by dCas9-Tet1 we designed 4 gRNAs targeting all 14 CpGs in the *Snrpn* promoter region. After infection with lentiviral vectors co-expressing dCas9-Tet1 and the 4 gRNAs for three days, some infection-positive cells as labeled by Cherry positive signal expressed from gRNA construct began to turn on GFP (Fig S2B). To assess the activation efficiency by dCas9-Tet1 with target gRNAs, we analyzed the cells infected by both viruses using FACS. Among the Cherry positive population, about 26% of cells with target gRNAs activated GFP, whereas only 1% of cells with a scrambled gRNA were GFP positive (Fig 1C and Fig S2C). These Cherry positive single cells were further cultured to allow for formation of ES cell colonies. Cells with target gRNAs, but not the scrambled gRNA, expressed GFP (Fig 1D). To confirm that the activation of GFP in these cells is caused by demethylation of the *Snrpn* promoter, we performed bisulfite sequencing of genomic DNA from these samples. As illustrated in Fig 1E and 1F, samples from cells with target gRNAs showed robust demethylation only in the *Snrpn* promoter region but not the adjacent *Dazl* locus, and samples from the cells with the scrambled gRNA showed a similar methylation status to the uninfected (Mock) control. We further analyzed the GFP-positive and -negative populations within infected Cherry-positive cells. As shown in Fig S2D, a more robust demethylation of the *Snrpn* promoter region was observed in double positive cells (Cherry+;GFP+). These results confirm the targeted erasure of DNA methylation by dCas9-Tet1 with gRNAs in proliferative cells.

b. De novo methylation of specific CpGs—To assess whether a dCas9-Dnmt3a fusion protein could *de novo* methylate promoter sequences and silence gene expression, we used cells carrying the Snrpn-GFP reporter in the *Gapdh* promoter. These cells are GFP positive because *Gapdh* is unmethylated and expressed in ES cells (Stelzer et al., 2015). We infected the Gapdh-Snrpn-GFP ESCs with lentiviruses expressing dCas9-Dnmt3a and gRNAs targeting the *Snrpn* promoter or a scrambled gRNA (Fig 2A and Fig S2E), followed by FACS analysis. Among infection-positive (Cherry positive) population, about 12% of cells with target gRNAs inactivated GFP, whereas only 2% of cells with the scrambled gRNA

were GFP negative (Fig 2B and S2F). When the Cherry positive cells were grown in culture, GFP expression of cells with target gRNAs remained off whereas cells with the scrambled gRNA and mock controls remained GFP positive (Fig 2C). Furthermore, bisulfite sequencing showed that transduction of dCas9-Dnmt3a/gRNAs resulted in a significant increase of DNA methylation in the *Snrpn* promoter region but not in the adjacent *Gapdh* region (Fig 2D and 2E). Further analysis of the GFP-positive and -negative populations within infected Cherry-positive cells showed a more robust methylation of the *Snrpn* promoter region in Cherry+;GFP- cells (Fig S2G). To overcome the possible limitation caused by low co-transduction efficiency of both dCas9-Dnmt3a and gRNA lentiviruses, a Doxycycline-inducible dCas9-Dnmt3a expression cassette was integrated into the Gapdh-Snrpn-GFP mES cell line by using a PiggyBac transposon system (Fig S2H). After delivery of the same group of target gRNAs, FACS analysis showed that GFP inactivation efficiency was increased to 25% (Fig 2F and S2I). Sorted Cherry-positive cells showed loss of GFP expression upon Doxycycline treatment (Fig 2G) and were robustly methylated in the *Snrpn* promoter region (Fig 2H). We also generated a new construct of dCas9-Dnmt3a-P2A-BFP which enables isolation of dCas9-Dnmt3a expressing cells by FACS. ~70% of GFP inactivation efficiency was achieved in FACS sorted double positive cells (BFP+;Cherry+) after lentiviral delivery of this construct together with gRNAs (Fig S2J).

In summary, our results indicate that the dCas9 fusion constructs described above either efficiently demethylate methylated sequences (dCas9-Tet1) or *de novo* methylate unmethylated sequences (dCas9-Dnmt3a) in dividing cells when targeted by specific guide RNAs.

Comparison of dCas9- and TALE-based methylation editing

To compare the methylation editing efficacy and effective range by dCas9-Tet1/Dnmt3a with TALE-based methods, we chose two previously reported loci edited by TALE-based method (Bernstein et al., 2015; Maeder et al., 2013) and designed a single gRNA targeting dCas9-Tet1/Dnmt3 to the same site bound by the TALE-Tet1/Dnmt3a. As shown in Fig S3A and S3C, dCas9-Dnmt3a with one single gRNA targeting the *p16* locus induced an average of 25% increase of methylation within a 320 bp region of the *p16* promoter whereas TALE-Dnmt3a only induced 13% increase within a 650 bp region. Similarly, dCas9-Tet1 with one single gRNA targeting the *RHOXF2* locus induced an average of 28% decrease of methylation within a 150 bp region of the *RHOXF2* promoter whereas TALE-Tet1 only induced 14% decrease within a 200 bp region (Fig S3B and S3C). These results suggest that dCas9-Tet1/Dnmt3a system has higher efficacy and resolution for methylation editing than TALE-based method.

To evaluate the specificity of dCas9-Tet1/Dnmt3a-mediated methylation editing, we performed dCas9 ChIP-seq assay and identified 9 binding sites in the presence of gRNAs targeting the *Dazl-Snrpn* region described in Fig S2A and 18 binding sites in the presence of gRNAs targeting CTCF binding sites adjacent to the *miR290* locus (see below Fig S6A). Fig S3D shows that among the identified binding sites for each group of gRNAs, the targeted locus (*Dazl-Snrpn* or *miR290*) showed the highest level of binding for dCas9-Dnmt3a (Table S1). The second and third strongest binding sites for each targeted locus were illustrated in

Fig S3E, and bisulfite sequencing analysis of these loci showed only marginal change in methylation level (Fig S3F and S3G), likely due to the significantly lower binding affinity of dCas9-Dnmt3a/Tet1 at these off-target loci compared to the targeted loci. These results indicate that dCas9-based epigenetic editing can be highly specific.

Targeted demethylation of *BDNF* promoter IV activates BDNF in neurons

DNA replication-independent active demethylation has been proposed to operate in post-mitotic neurons (Guo et al., 2011; Martinowich et al., 2003). To test whether active demethylation can be induced in post-mitotic neurons, we applied the dCas9-Tet1 system to study the regulation of the *BDNF* gene. BDNF expression can be induced by neuronal activity accompanied by demethylation of its promoter IV (Chen et al., 2003; Martinowich et al., 2003). We designed 4 gRNAs targeting 11 CpGs in *BDNF* promoter IV (Fig S4A) to determine whether dCas9-Tet1 can activate BDNF by inducing demethylation of this promoter (Fig 3A). Mouse cortical neurons were isolated from E17.5 embryos and cultured for two days *in vitro* (DIV2) following a well-established experimental procedure for producing primary neuronal culture (Ebert et al., 2013). As shown in Fig S4B–D, KCl treatment induced BDNF expression in these neurons with no detectable cell proliferation. Neurons at day 3 in culture (DIV3) were infected with lentiviral vectors expressing dCas9-Tet1 with or without the 4 gRNAs at almost 100% transduction efficiency (Fig S4E). At 48-hour post infection some of the cultures were treated with KCl to induce neuronal activity. As shown in Fig 3B and 3C, dCas9-Tet1/gRNAs induced BDNF expression by about 6-fold, whereas dCas9-Tet1 in the absence of gRNAs showed only a slight induction (less than 2-fold) and a catalytically dead form of Tet1 (dC-dT) showed no induction. Importantly, the same group of dCas9-Tet1/gRNAs did not induce *Npas4* expression (Fig S4F), another neuronal activity-inducible gene (Lin et al., 2008). Co-transduction of dCas9-Tet1 with each individual gRNA targeting the *BDNF* promoter IV showed a 2–3 fold induction of BDNF (Fig S4G). We performed bisulfite sequencing to examine the methylation state of *BDNF* promoter IV. As shown in Fig 3D and 3E, dCas9-Tet1/gRNAs significantly reduced methylation in this region in contrast to gRNA negative controls while KCl treatment also induced demethylation of CpGs at positions of −148, −66 and 19 (relative to transcription start site).

Our results demonstrate that demethylation of the *BDNF* promoter IV can be induced by dCas9-Tet1/gRNAs and is sufficient to activate BDNF expression. Because post-mitotic neurons were used for these experiments, loss of methylation was likely due to active demethylation. To further support this conclusion, we examined 5-hmC level in the *BDNF* promoter IV during the time course of dCas9-Tet1 induced demethylation by Tet-assisted Bisulfite sequencing (TAB-seq) analysis. As shown in Fig S4H, 5-hmC was detected 40-hour post infection with dCas9-Tet1 and gRNA lentiviruses and diminished after 60 hours. Similarly, 5-hmC was also detected after KCl treatment (Fig S4I). As bisulfite sequencing method does not distinguish unmethylated 5-cytosine (5-C) and 5-formlycytosine/5-carboxylcytosin (5-fC/5-caC) generated from 5-hmC, it is possible that some CpGs were 5-fC/5-caC modified after targeting with dCas9-Tet1/gRNA. Nevertheless, inhibition of the base excision repair pathway by treatment with ABT-888 (an inhibitor of PARP) reduced the

activation of BDNF by KCl treatment (Fig S4J), suggesting that demethylation of *BDNF* promoter IV contributes to BDNF activation.

To test whether endogenous Tet activity was required to regulate BDNF expression upon neuronal activity stimulation, we treated DIV3 neurons with 2-hydroxygluterate, a competitive inhibitor for α-ketoglutarate-dependent dioxygenases including Tet enzymes (Xu et al., 2011). As shown in Fig S4K, pharmacological inhibition of Tet enzymatic activity completely abolished the induction of BDNF expression by KCl treatment. Furthermore, mouse primary cortical neurons carrying a Tet1 null mutant showed significantly attenuated activation kinetics of BDNF (Fig S4L), supporting a role of endogenous Tet for induction of neuronal activity.

Targeted demethylation of the *MyoD* distal enhancer facilitates myogenic reprogramming of fibroblasts

The role of MyoD as a master regulator for muscle development was initially defined by the observations that demethylation of DNA in fibroblasts by 5-Aza (5-Aza-2'-deoxycytidine) treatment resulted in activation of MyoD and subsequent myoblast conversion and myotube formation (Constantinides et al., 1977; Davis et al., 1987; Lassar et al., 1986). Six muscle-specific DMRs have been described within the 50 kb upstream region of *MyoD* gene (Schultz et al., 2015), and DMR-5 overlaps with a known distal enhancer of *MyoD* (Brunk et al., 1996) as shown in Fig 4A. To test whether demethylation of DMR-5 would activate MyoD in fibroblasts, we designed 4 gRNAs targeting this DMR (Fig S5A). Co-expression of dCas9-Tet1 with these gRNAs in C3H10T1/2 cells, a sub-clone from mouse embryonic fibroblasts previously used for 5-Aza mediated MyoD activation (Constantinides et al., 1977), resulted in a moderate induction of MyoD expression (3-fold) as shown in Fig 4B. Combination of dCas9-Tet1/*MyoD* DMR-5 gRNAs with 5-Aza treatment resulted in a higher induction of MyoD as shown in Fig S5F. Bisulfite sequencing showed a substantial reduction of methylation in the DMR-5 region of sorted infection-positive cells transduced with dCas9-Tet1 and target gRNAs lentiviruses, but not with a catalytically dead Tet1 (dC-dT) or a scrambled gRNA (Fig 4C and 4D). To investigate whether demethylation of the *MyoD* distal enhancer region could reprogram fibroblasts into muscle cells, we infected C3H10T1/2 cells with lentiviruses expressing dCas9-Tet1 and gRNAs. The cells were cultured for 14 days and analyzed for MyoD and MHC (Myosin Heavy chain, a myotube specific marker) expression. As shown in Fig 4E and 4F, co-expression of dCas9-Tet1 with gRNAs targeting DMR-5 induced a moderate expression level of MyoD, but was not sufficient to induce myotube formation in the absence of 5-Aza treatment.

We then investigated whether targeted demethylation of DMR-5 would synergize with 5-Aza treatment to induce myotube formation (Fig S5B). To follow the process of myotube formation after 5-Aza treatment, a time-course experiment was performed. Multi-nucleated myotube (MHC-positive) with heterogeneous sizes began to form 14 days post treatment, and both MyoD-positive cell ratio and myotube density and size then increased up to day-25 (Fig S5C–E). Co-expression of dCas9-Tet1 with gRNAs targeting *MyoD* DMR-5 facilitated the myotube formation 14 days post-treatment as evidenced by significantly more mature, multi-nucleated MHC+ clusters (>2 nuclei per MHC+ cluster) compared to cells expressing

only dCas9-Tet1 or dC-dT with *MyoD* DMR-5 gRNAs (Fig 4E, 4G, and 4H). A similar observation was made when the cells were analyzed at a later time point (16-day) post-treatment (Fig S5G–J). Our results suggest that demethylation of the *MyoD* distal enhancer by dCas9-Tet1/gRNA synergizes with 5-Aza in C3H10T1/2 cells to substantially facilitate myoblast conversion and myotube formation.

Targeted *de novo* methylation of CTCF binding sites alters CTCF-mediated chromatin loops

CTCF is a highly conserved zinc finger protein that plays a primary role in the global organization of chromatin architecture (Phillips and Corces, 2009). Transcriptional enhancers normally interact with their target genes through the formation of DNA loops (Gibcus and Dekker, 2013; Gorkin et al., 2014; Kagey et al., 2010), which typically are constrained within larger CTCF-mediated loops called insulated neighborhoods (Dowen et al., 2014; Ji et al., 2016; Phillips-Cremins et al., 2013), which in turn can form clusters of loops that contribute to topologically associating domains (TADs) (Dixon et al., 2012; Nora et al., 2012). Deletion of the CTCF loop anchor sites of insulated neighborhoods can cause enhancers to interact inappropriately with genes located outside the loop and thus increase their expression (Dowen et al., 2014). Interestingly, methylation of the DNA recognition site of CTCF has been reported to block CTCF binding (Bell and Felsenfeld, 2000; Wang et al., 2012). To study whether methylation of specific CTCF sites could alter CTCF-mediated chromatin loops, we applied the dCas9-Dnmt3a system to target CTCF anchor sites (Fig 5A). We designed specific gRNAs (Fig S6) targeting dCas9-Dnmt3a to two CTCF sites to investigate whether *de novo* methylation would interfere with the looping function of CTCF (Fig 5B and 5F). Doxycycline-inducible dCas9-Dnmt3a mES cells (Fig S2H) were infected with lentiviruses expressing the gRNAs and transduced cells were FACS sorted for subsequent analysis.

Targeting of dCas9-Dnmt3a to the CTCF binding site bordering the *miR290* loop that harbors a super-enhancer (Fig 5B) induced *de novo* methylation of CpGs at this site (Fig 5D and 5E). Gene expression analysis of transduced cells showed a significant elevation of *Nlrp12* gene, which is outside of this super-enhancer-containing insulated neighborhood and next to the targeted CTCF site, but did not affect the expression of genes that are located inside the *miR290* loop or of genes in other neighboring loops including *AU01801* and *Myadm* (Fig 5C). Similarly, targeting of dCas9-Dnmt3a to the CTCF binding site bordering the *Pou5f1* gene loop that harbors another super-enhancer (Fig 5F) induced methylation of CpGs in the CTCF binding sequence (Fig 5H and 5I), and increased the expression of H2Q10, which is located in a neighboring loop and next to the targeted CTCF site, but did not affect the expression of *Pou5f1* gene itself or *Tcf19* gene in the other neighboring loop (Fig 5G). For either targeted CTCF sites, a catalytically inactive Dnmt3a form (dC-dD) did not induce changes in methylation level or gene expression as did by dC-D (Fig 5C–E, and 5G–I). These observations are consistent with the results obtained when these CTCF sites were deleted (Dowen et al., 2014), and support the notion that methylation of the CTCF binding site interferes with its insulator function.

To test whether targeted methylations of CTCF binding sites would result in increased interaction frequencies between insulated super-enhancers and activated genes, Chromosome Conformation Capture (3C) assay was performed at these loci. As shown in Fig 6A, the interaction frequency between super-enhancers in the *miR290* loop and the newly activated gene (*Nlrp12*) in the neighboring loop was significantly increased but the interaction between *Nlrp12* and *Myadm* genes remained the same, indicating an open conformation for this targeted CTCF loop. To confirm that the increased interaction frequency was due to blocking CTCF anchoring, we performed a CTCF ChIP assay. Binding of CTCF to the targeted genomic site was significantly reduced in the sample with *miR290* target gRNAs as compared to the sample with a scrambled gRNA, gRNAs targeting other CTCF binding sites or a catalytically inactive dC-dD with *miR290* target gRNAs (Fig 6B), supporting the notion that DNA methylation blocks CTCF anchoring and thus alters the CTCF loop conformation. A similar set of experiments was performed for the second CTCF loop (*Pou5f1* loop) demonstrating increased interaction frequency between the insulated super-enhancers and the newly activated gene (*H2Q10*), and decreased binding of CTCF after targeted methylation of its binding site (Fig 6C and 6D).

In summary, our results demonstrate that the dCas9-Dnmt3a system can be used to change the methylation state of specific CTCF anchor sites and thus to interfere with the CTCF looping function.

In vivo demethylation of an endogenous locus for gene activation by dCas9-Tet1

To test whether the dCas9-mediated DNA methylation-editing tools could be used to alter methylation *in vivo* we utilized a methylation sensitive reporter mouse previously generated (Fig 7A, Stelzer et al, *Cell Reports*, 2016, in press). In these transgenic mice, a methylation sensitive Snrpn-GFP cassette was inserted into the *Dlk1-Dio3* locus to report the methylation status of its intergenic-differentially methylated region (IG-DMR). As the IG-DMR of this locus acquires paternal methylation during spermatogenesis, the GFP reporter (IG-DMR$^{GFP/Pat}$) is constitutively repressed in heterozygous mice carrying the paternal Snrpn-GFP allele (Stelzer et al., *Cell Reports*, 2016, in press). As shown above the GFP reporter in the *Dazl* locus was activated by targeted promoter demethylation in mES cells (Fig 1). To assess whether the *Dlk1-Dio3* locus GFP reporter could be activated by dCas9-Tet1 in differentiated cells we derived adult mouse skin fibroblast cells from the tails of IG-DMR$^{GFP/Pat}$ transgenic mice, which were then transduced by lentiviruses expressing dCas9-Tet1 with *Snrpn* target gRNAs or a scrambled gRNA, or a catalytically dead form of Tet1 (dC-dT) with *Snrpn* target gRNAs (Fig 7A). The results in Fig 7B and 7C reveal GFP reporter activation in about 80% of Cherry (gRNA) positive fibroblasts but only when transduced by both dCas9-Tet1 and *Snrpn* gRNAs lentiviruses. FACS analysis of these cells further confirmed this notion (Fig S7A–C).

To investigate whether the DNA methylation status can be modified *in vivo*, we infected 3 epidermal sites on the ventral side of an IG-DMR$^{GFP/Pat}$ transgenic mouse with the dCas9-Tet1 and *Snrpn* gRNAs (Fig S7D). Cells were sparsely infected with cherry expression seen only in some of the hair follicles. dCas9-Tet1 with *Snrpn* gRNAs, but not dCas9-Tet1 with the scrambled gRNA or dC-dT with *Snrpn* gRNAs, was able to activate GFP reporter

expression in about 85% infected skin dermal cells *in vivo* (Fig 7H, S7E&F). In addition we infected the brain of an IG-DMR$^{GFP/Pat}$ transgenic mouse with lentiviral vectors using a stereotaxic setup and analyzed the effect on targeted DNA methylation in brain slices by confocal microscopy. To eliminate possible inter-individual variability, we injected lentiviral vectors expressing dCas9-Tet1 and *Snrpn* gRNAs, as well as the two negative control vector combinations into different regions of the same brain (Fig 7D). As shown in Fig 7E&F, after infection with all three lentiviral combinations as indicated by Cherry expression, only lentiviral vectors expressing dCas9-Tet1 with *Snrpn* gRNAs, but not vectors expressing dCas9-Tet1 with sc gRNA or dC-dT with *Snrpn* gRNAs, activated the GFP reporter with an activation efficiency of about 70% (Fig 7G).

DISCUSSION

In this study we have repurposed the CRISPR/Cas9 system to edit the methylation status of genomic sequences. The catalytically inactive Cas9 protein (dCas9) was fused either to the catalytic domain of Tet1 (dCas9-Tet1) or to Dnmt3a (dCas9-Dnmt3a) to predictably alter the epigenetic state of target sequences. A GFP reporter inserted into the promoter region of the methylated and silenced *Dazl* gene was demethylated and activated when targeted by dCas9-Tet1 whereas the GFP reporter inserted into the promoter region of the active and unmethylated *Gapdh* gene was *de novo* methylated and silenced when targeted by dCas9-Dnmt3a. When the dCas9-Tet1 was targeted to the inactive *BDNF* promoter IV in post-mitotic neurons, the promoter became demethylated and activated. Importantly, this tool predictably altered the methylation state and activity of regulatory regions: Targeted demethylation of the inactive distal enhancer of *MyoD* activated the gene and facilitated muscle differentiation and targeted methylation of CTCF anchor sites inhibited CTCF binding and interfered with its function as an insulator between chromatin loops. Finally, the editing tools can *in vivo* alter the methylation state of regulatory sequences as injection of the lentiviral vectors of dCas9-Tet1 with target gRNAs into the dermis or brain of transgenic mice demethylated the methylated *Snrpn* promoter in the *Dlk1-Dio3* imprinted locus and activated the methylation-sensing GFP reporter.

Dynamic DNA methylation has been proposed to decode neuronal activities (Sweatt, 2013). For instance, treatment of neurons with KCl has been shown to de-silence promoter IV of *BDNF* and induce BDNF expression associated with demethylation of some methylated CpGs in the promoter region (Chen et al., 2003; Martinowich et al., 2003). When the *BDNF* promoter IV was targeted by dCas9-Tet1, extensive demethylation of methylated CpGs was observed, and BDNF was activated to a similar level as when the cultures were treated with KCl. Because the neurons were post-mitotic, the dCas9-Tet1-mediated demethylation of the promoter sequences was likely the result of active demethylation as has been proposed previously (Wu and Zhang, 2014). Although it is possible that some CpGs in the *BDNF* promoter were 5-fC/5-caC modified after targeting with dCas9-Tet1/gRNA, blocking restoration of 5-fC/5-caC into unmethylated cytosine by inhibition of the BER pathway reduced *BDNF* expression, suggesting that demethylation of the *BDNF* promoter IV contributes to the activation of *BDNF*. Importantly, our results establish a causal relationship between demethylation of *BDNF* promoter IV and gene activation.

The role of DNA methylation as a barrier between cell lineages is consistent with the previous observation that demethylation of DNA in fibroblasts by treatment with 5-Aza can activate MyoD and mediate myotube formation (Constantinides et al., 1977). Targeting of dCas9-Tet1 to the methylated distal enhancer of *MyoD* in fibroblasts induced demethylation of CpGs and resulted in a moderate activation of *MyoD* but failed to generate myoblasts. However, when dCas9-Tet1/gRNA lentiviral transduction was combined with 5-Aza treatment, a significantly enhanced myoblast and myotube formation was observed as compared to 5-Aza treatment alone. It is possible that demethylation of the additional DMRs in combination with the distal enhancer may be required to induce efficient conversion of fibroblasts to myoblasts.

Recent studies of mammalian chromosome structure reveal that chromatin is organized in topologically associating domains and gene loops mediated by chromatin architecture proteins such as Cohesin and CTCF (Dekker and Mirny, 2016). Emerging data suggest that higher-order chromatin structures confer epigenetic information during development and are frequently altered in cancer (Ji et al., 2016; Narendra et al., 2015). It has been reported that binding of CTCF is inhibited when its recognition sequence is methylated (Bell and Felsenfeld, 2000; Wang et al., 2012). Targeting of dCas9-Dnmt3a to two CTCF binding sites induced *de novo* methylation of CpGs in these sites and interfered with the insulator function of the protein as evidenced by increased interaction frequencies between insulated super-enhancers in the targeted loop and genes in the neighboring loop causing up-regulation of these genes. This suggests that the dCas9-Dnmt3a system is a useful tool to manipulate chromatin structure and to assess its functional significance during development and in disease context.

Our results indicate that dCas9 fused to the epigenetic effectors Tet1 and Dnmt3a represent a powerful toolbox to edit DNA methylation of specific genomic sequences. Comparison of these tools with TALE-based method showed a higher efficacy and resolution for methylation editing, and dCas9 ChIP-seq followed by bisulfite sequencing of potential off-target binding loci revealed marginal changes in methylation levels, suggesting that high specificity can be achieved with properly designed gRNAs. During the preparation of our manuscript, Vojta et al. also reported that dCas9 fused with Dnmt3a can be used to methylate two human gene promoters (Vojta et al., 2016), and Xu et al. and Choudhury et al. reported that dCas9 fused with Tet1 can be used to demethylate gene promoters (Choudhury et al., 2016; Xu et al., 2016). Therefore, these dCas9-Dnmt3a/Tet1 tools will be useful to gain insight into the functional significance of DNA methylation in diverse biological processes such as gene expression, cell fate determination, and organization of high-order chromatin structures.

Methods and Resources (6 sub-sections)

CONTACT FOR REAGENT AND RESOURCE SHARING

Further information and requests for reagents may be directed to, and will be fulfilled by the corresponding author Rudolf Jaenisch (jaenisch@wi.mit.edu)

EXPERIMENTAL MODEL AND SUBJECT DETAILS

Mouse lines and breeding strategies—Tet1 mutant mice were previously generated in our lab (Dawlaty et al., 2011). Tet1 KO mice in the study were maintained in a mixed 129 and C57BL/6 background. To obtain Tet1 KO mice, male and female mice heterozygous for Tet1 were crossed. To obtain wild type mouse primary cortical neurons, male and female C57BL/6 mice were mated. IG-DMR$^{GFP/Pat}$ methylation reporter mouse line was generated as described (Ref: Stelzer et al., Parent-of-origin DNA methylation dynamics during mouse development, *Cell Report*, in press). Male mice with IG-DMR$^{GFP/Pat}$ reporter allele were crossed with C57BL/6 females to generate adult offsprings carrying the paternally transmitted allele for *in vivo* DNA methylation editing analysis. Mice were handled in accordance with institutional guidelines and approved by the Committee on Animal Care (CAC) and Department of Comparative Medicine (DCM) of Massachusetts Institute of Technology.

Mouse primary cortical neuron culture, EDU labeling and neural induction—Dissociated E17.5 cortical neuron cultures were generated from wild type or Tet1 KO mouse embryos as described previously (Ebert et al., 2013). Briefly, E17.5 cortices were dissected in ice-cold 1 X HBSS (Gibco 14185-052) containing 1 x pen/strep (Gibco: 15140122), 1 x pyruvate (Gibco: 11360070) and 30 mM Glucose. Tissues were minced into around 1 mm^3 and dissociated with Papain neural tissue dissociation system (Worthington Biochemicals) following the manufacturer's instruction. Cells were resuspended in NM5 media (%5 FBS (Hyclone), 2% B27 supplement (Gibco 17504044), 1 x pen/strep and 1 x glutamax I (Gibco 35050-061)). 1 x 10^6 cells were plated per well of a 6-well plate coated with poly-D-lysine (PDL, Sigma). On DIV2, cells were treated with 2.5 uM AraC overnight (Sigma C-6645) to eliminate the excessive cell division of mitotic astrocytes and neural progenitor cells. Cultures were fed at DIV3 with fresh NM5 media and subsequently membrane depolarized with 50 mM KCl or infected with preferred lentivirus. We started the treatment at the very beginning of the *in vitro* culture so the step of AP5 and TTX (tetrodotoxin) treatment to silence basal activity in the culture before KCl treatment was omitted. For EDU labeling, primary neuronal culture were treated with EDU at a final concentration of 10 uM for 24 hours followed by Click-it EDU labeling procedure according to the manufacturer's instruction (Thermo Fisher Scientific). Cells were fixed for immunohistochemical analysis, lysed in Trizol to extract total RNA for RT-qPCR or lysed to extract DNA for bisulfite sequencing analysis.

METHOD DETAILS

Plasmid design and construction—PCR amplified Tet1 catalytic domain from pJFA344C7 (Addgene plasmid: 49236), Tet1 inactive catalytic domain from MLM3739 (Addgene plasmid: 49959), or Dnmt3a from pcDNA3-hDNMT3A (Addgene plasmid: 35521) were cloned in modified pdCas9 plasmid (Addgene plasmid: 44246) with BamHI and EcoRI sites. Then dCas9-NLS-Tet1 or dCas9-NLS-Dnmt3a were PCR amplified and cloned into FUW vector (Addgene plasmid: 14882) with AscI and EcoRI to package lentiviruses. NLS-dCas9-NLS-Tet1 was cloned by inserting annealed oligos (NLS) into FUW-dCas9-NLS-Tet1 with XbaI and AscI. The gRNA expression plasmids were cloned by inserting annealed oligos into modified pgRNA plasmid (Addgene plasmid: 44248) with

AarI site. The PiaggyBac-dCas9-Tet1 and -dCas9-Dnmt3a were cloned by ligation of PCR-amplified dCas9-NLS-Tet1 or dCas9-NLS-Dnmt3a from FUW constructs with modified PiggyBac transposon vector (Wilson et al., 2007) with NheI and EcoRI. All constructs were sequenced before transfection. Primer information for gRNA design and construction is listed in Supplemental Table S2. Related plasmids have been deposited into Addgene plasmid database. TALE-Dnmt3a construct targeting *p16* locus is a gift from Dr. Klaus Kaestner, and TALE-Tet1 targeting *RHOXF2* locus is from Addgene (Plasmid #49943). Full length protein sequences of dCas9-Dnmt3a and dCas9-Tet1CD and their mutants are listed in Supplemental Table S6.

Cell culture, lentivirus production, and stable cell line generation—Mouse embryonic stem cells (mESCs) were cultured on irradiated mouse embryonic fibroblasts (MEFs) with standard ESCs medium: (500 ml) DMEM supplemented with 10% FBS (Hyclone), 10 ug recombinant leukemia inhibitory factor (LIF), 0.1 mM β-mercaptoethanol (Sigma-Aldrich), penicillin/streptomycin, 1 mM L-glutamine, and 1% nonessential amino acids (all from Invitrogen). C3H10T1/2 cells were cultured in standard DEME medium with 10% FBS. Lentiviruses expressing dCas9-Tet1, dCas9-Dnmt3a, and gRNAs were produced by transfecting HEK293T cells with FUW constructs or pgRNA constructs together with standard packaging vectors (pCMV-dR8.74 and pCMV-VSVG) followed by ultra-centrifugation-based concentration. Virus titer (T) was calculated based on the infection efficiency for 293T cells, where T = (P*N) / (V), T = titer (TU/ul), P = % of infection positive cells according to the fluorescence marker, N = number of cells at the time of transduction, V = total volume of virus used. Note TU stands for transduction unit. To generate stable cell lines with integrated Doxycycline-inducible dCas9-Tet1 or dCas9-Dnmt3a transgenes, PiggyBac-dCas9-Tet1 or -dCas9-Dnmt3a construct, with a helper plasmid expressing transposase, were transfected into C3H10T1/2 cell using X-tremeGENE 9 transfection reagent (Roche) or into mESCs cells using Xfect transfection reagent (Clontech), according to the provider's protocol. Stably integrated cells were selected with G418 (400 ug/ml) for 10 days. Adult mouse fibroblasts were derived from tails of IG-DMR$^{GFP/Pat}$ reporter mice. Briefly, ~ 2 cm-long mouse tail was obtained from 3 month old mouse carrying paternally transmitted IG-DMR-Snrpn-GFP methylation reporter, and sterilized by 70% EtOH. ~ 2 mm x 2 mm minced tail pieces were digested with 5 ml of 1mg/ml Collagenase IV at 37°C for 90 min in a 15 ml Falcon tube. 5 ml MEF medium were added into the tube to terminate the digestion. Dissociated cells were extruded through a 40 um cell strainer with gentle grind using a syringe plug. Cells were then collected and cultured for viral infection. Cells were analyzed 3 days post-infection in this study.

Viral infection of mice and tissue sample preparation—Mice were infected with appropriate lentiviral cocktails in accordance with institutional guidelines and approved by the Committee on Animal Care (CAC) and Department of Comparative Medicine (DCM) of Massachusetts Institute of Technology. Specifically, to infect mouse skin, lentiviruses expressing dCas9-Tet1 with sc gRNA, an inactive mutant of dC-dT with target gRNAs, and dCas9-Tet1 with target gRNAs were delivered by Hamilton syringe into multiple dermal sites on the ventral side of the deeply anesthetized mouse carrying the Paternal IG-DMR^{GFP} reporter allele (Fig S7D). To infect mouse brain, various lentiviral mixtures were delivered

by stereotaxic setup (Leica BIOSYSTEMS, BenchMark Digital Stereotaxic with Manual Fine Drive) into the following locations (relative to the Franklin and Paxinos mouse brain atlas) of the deeply anesthetized mouse carrying the paternal IG-DMR$^{GFP/Pat}$ reporter allele (Fig 7D): dCas9-Tet1 with sc gRNA (A-P 0.70mm, M-L 1.50mm, D-V 1.50mm), an inactive mutant of dC-dT with *Snrpn* gRNAs (A-P −1.90mm, M-L −1.50mm, D-V 1.50mm), and dCas9-Tet1 with *Snrpn* gRNAs (A-P −1.90mm, M-L 1.50mm, D-V 1.50mm). The titers for dC-T/dC-dT and gRNA lentiviruses are 1.2 x 10^4 TU/ul and 1.2 x 10^5 TU/ul respectively. Mice were sacrificed 3 days after infection. The animals were fixed by transcardial perfusion with 4% paraformaldehyde (PFA)/PBS. Fixed skin pads and brain samples were dissected and post fixed with 4% paraformaldehyde (PFA)/PBS overnight at 4 °C. The brain samples were sectioned with a vibratome (Leica VT1100) at 150 um thickness and the skin samples were sectioned with a cryostat (Leica) at 10 um thickness followed by immunohistochemical analysis. For vibratome sectioning, tissues were embedded in 3% agarose gel. For cryosectioning, tissues were equilibrated in 30% sucrose/PBS prior to embedding in Optimal Cutting Temperature (OCT) compound.

Immunohistochemistry, microscopy, and image analysis—Neurons, HEK293T cells, mouse ES cells and C3H10T1/2 cells were fixed with 4% paraformaldehyde (PFA) for 10 min at room temperature. Cells were permeablized with PBST (1 x PBS solution with 0.1% Triton X-100) before blocking with 10% Normal Donkey Serum (NDS) in PBST. Cells were then incubated with appropriately diluted primary antibodies in PBST with 5% NDS for 1 hours at room temperature or 12 hours at 4 °C, washed with PBST for 3 times at room temperature and then incubated with desired secondary antibodies in TBST with 5% NDS and DAPI to counter stain the nuclei. Cells were washed 3 times with PBST before mounted onto slides with Fluoromount G (SouthernBiotech). Immunostaining procedures for tissue sections were previously described (Wu et al., 2014a). Briefly, sections were permeablized with PBST (1 x PBS solution with 0.5% Triton X-100) for 1 hour at RT before blocking with 10% Normal Donkey Serum (NDS) in PBST. Slices were then incubated with desired primary antibodies in PBST with 5% NDS for 24 hours at 4 °C, washed with PBST for 3 times at room temperature and then incubated with secondary antibodies in TBST with 5% NDS and DAPI to counter stain the nuclei. Sections were washed 3 times with PBST before slide mounting. The following antibodies were used in this study: Chicken anti-GFP (1:1000, Aves Labs), Mouse anti-Cas9 (7A9, 1:1000, Active Motif), Rabbit anti-BDNF (1:1000, Thermo Fisher), Chicken anti-MAP2 (1:1000, Encor Biotech), Mouse anti-MAP2 (1:1000, Sigma-Aldrich), Mouse anti-Tuj1 (1:1000, Biolegend), Rabbit anti-MyoD (C-20, 1:1000, Santa Cruz Biotechnology), Mouse anti-MHC (MF20, 1:1000, R&D systems), Mouse anti-MyoG (F5G, 1:1000, Thermo Fisher). Images were captured on a Zeiss LSM710 confocal microscope and processed with Zen software, ImageJ/Fiji, and Adobe Photoshop. For imaging based quantification, unless otherwise specified, 3–5 representative images were quantified and data were plotted as mean ± SD with Excel or Graphpad.

FACS analysis—To assess the proportion of GFP and/or Cherry positive cells after treatment, the treated cells were dissociated with trypsin and single-cell suspensions were prepared in growth medium subject to a BD FACSAria cell sorter according to the

manufacture's protocol at the Whitehead Institute Flow Cytometry Core. Data were analyzed with FlowJo software.

Fibroblast-to-myoblast conversion assay—Myoblast conversion assay was described previously (Constantinides et al., 1977). Briefly, C3H10T1/2 mouse embryonic fibroblast cells were plated as 1 x 10^4 cells per well in 6-well plate, and then infected with lentiviruses expressing dCas9-Tet1 and target gRNAs. 24-hour post infection, cells were treated with vehicle control (HEPES buffer) or 5-Azacytidine (1 uM) for 24-hour, and harvested at different time points for subsequently analysis. DMRs upstream of mouse *MyoD* gene were defined based on human/mouse genome homology (Schultz et al., 2015).

Western blot—HEK293T cells were transfected with various constructs by X-tremeGENE 9 reagent following manufacturer's protocol. 2-day post transfection, cells were lysed by RIPA buffer with proteinase inhibitor (Invitrogen), and subject to standard immunoblotting analysis. Mouse anti-Cas9 (1:1000, Active Motif) and mouse α-Tubulin (1:1000, Sigma) antibodies were used.

RT-qPCR—Cells were harvested using Trizol followed by Direct-zol (Zymo Research), according to manufacturer's instructions. RNA was converted to cDNA using First-strand cDNA synthesis (Invitrogen SuperScript III). Quantitative PCR reactions were prepared with SYBR Green (Invitrogen), and performed in 7900HT Fast ABI instrument. Primer information for RT-qPCR is listed in Supplemental Table S3.

ChIP assay—ChIP experiment was performed as previously described (Dowen et al., 2014). Briefly, cells were cross-linked by 1% formaldehyde in the medium for 10 min in room temperature, and then quenched by adding 0.125 M Glycine for 5 min. Collected cells were washed with PBS twice, and then re-suspended in 3.5 ml of sonication buffer. Sonication was performed for 10 cycles with 0.5 min pulse on and 1 min rest, and 24 watts in ice-water mixture. Then cell lysate was spun down with 14,000 x rpm for 10 min at 4 °C. 50 ul of supernatant was saved as input for gDNA. 10 ul of anti-CTCF antibody (EMD Millipore: 07729) or anti-Cas9 antibody (Active Motif) was added and incubate overnight at 4 °C. 50 ul protein G dynabeads was added into antibody-cell lysate mixture and incubate overnight at 4 °C. Then beads were washed with sonication buffer, sonication buffer with high salt (500 mM NaCl), LiCl wash buffer, and TE buffer. Bound protein-DNA complex was eluted from beads by incubation in a 65 °C oven for 15 min, and then reverse cross-linked under 65 °C over-night. The bound DNA was purified with Qiagen QIAquick PCR Purification Kit, and then subject to qPCR analysis or sequencing.

ChIP-seq data analysis—Sequencing data was analyzed with a previously reported method (Wu et al., 2014b). Reads are demultiplexed and the first 25 bases are mapped to mouse genome (mm10) using STAR (Dobin et al., 2013), requiring unique mapping allowing one mismatch. Mapped reads are collapsed and the same number of reads (about 15 million) are randomly sampled from each sample to match sequencing depth. Peaks are called using MACS (Zhang et al., 2008) with default settings. For each sample, the other five samples are each used as a control and only peaks called over all five controls are defined as candidate peaks. Candidate peaks are filtered by fold of enrichment over background and the

threshold is chosen such that no peaks pass this threshold in the four control samples (input, mock IP, dCas9 alone, and scrambled gRNA). Note that six candidate peaks in input mapped to 45S rRNA and mitochondria DNA are excluded from the analysis. Raw data is available in the following link: http://www.ncbi.nlm.nih.gov/geo/query/acc.cgi?token=ktohskmgnhudhud&acc=GSE83890

Bisulfite Conversion, PCR and Sequencing—Bisulfite conversion of DNA was established using the EpiTect Bisulfite Kit (Qiagen) following the manufacturer's instructions. The resulting modified DNA was amplified by first round of nested PCR, following a second round using loci specific PCR primers (Supplemental Table S3). The first round of nested PCR was done as follows: 94 °C for 4 min; 55 °C for 2 min; 72 °C for 2 min; Repeat steps 1–3 1 X; 94 °C for 1 min; 55 °C for 2 min; 72 °C for 2 min; Repeat steps 5–7 35X; 72 °C for 5 min; Hold 12 °C. The second round of PCR was as follows: 95 °C for 4 min; 94 °C for 1 min; 55 °C for 2 min; 72 °C for 2 min; Repeat steps 2–4 35 X; 72 °C for 5 min; Hold 12°C. The resulting amplified products were gel-purified, sub-cloned into a pCR2.1-TOPO-TA cloning vector (Life technologies), and sequenced. Primer information for bisulfite sequencing is listed in Supplemental Table S4.

Locus-specific TAB-seq—TAB-Seq was performed as described previously (Yu et al., 2012). Briefly, 1 ug of genomic DNA from treated mouse cortical neuron was glucosylated in a solution containing 50 mM HEPES buffer (pH 8.0), 25 mM MgCl2, 100 ng/ml model DNA, 200 mM UDP-Glc, and 1 mM bGT at 37C for 1 hr. After the reaction, the DNA was column purified. The oxidation reactions were performed in a solution containing 50 mM HEPES buffer (pH 8.0), 100 mM ammonium iron (II) sulfate, 1 mM a-ketoglutarate, 2 mM ascorbic acid, 2.5 mM DTT, 100 mM NaCl, 1.2 mM ATP, 15 ng/ml glucosylated DNA, and 3 mM recombinant mTet1. The reactions were incubated at 37C for 1 hr. After proteinase K treatment, the DNA was column purified and then applied to EpiTect Bisulfite Kit (QIAGEN) following the supplier's instruction. The resulting modified DNA was amplified by first round of nested PCR, following a second round using loci specific PCR primers (Supplemental Table S3). The resulting amplified products were gel-purified, sub-cloned into a pJET cloning vector (Life technologies), and sequenced. Primer information for bisulfite sequencing is listed in Supplemental Table S4.

Chromosome Conformation Capture (3C) assay—5 x 10^6 mESCs were fixed with 1% formaldehyde for 20 min at room temperature, and the reaction was quenched by 0.125 M glycine for 5 min at room temperature. Cross-linked cells were collected and washed with 1 ml ice cold PBS. Cell pellet was re-suspended with 550 μl lysis buffer (10 mM Tris-HCl with pH 8.0, 10 mM NaCl, and 0.2% IGEPAL CA630 with proteinase inhibitor), and incubated on ice for 20 min. Cell pellet was then washed twice with 1 x NEB buffer 2 (NEB, B7002S), then incubated with 50 μl 0.5% SDS for 10 min at 62 °C. After heating, 145 μl H_2O and 25 μl 10% Triton X-100 were added into the mixture and incubate for 15 min at 37 °C. 25 μl 10 x NEB buffer 2 and 100 U BglII (NEB, R0144S) were added to digest chromatin over night at 37 °C. The digest reaction was inactivated by incubation for 20 min at 62 °C. Then 713 μl H2O, 120 μl 10 x T4 DNA ligase buffer (NEB, B0202), 100 μl 10% Triton X-100, 12 μl 10 mg/ml BSA, and 5 μl T4 DNA ligase (NEB, M0202) were added and

incubated for 22 hour at 16 °C. The chromatin was reverse cross-linked, and DNA was purified by phenol:chloroform:isoamyl alcohol (Sigma, P3803) extraction. The 3C interactions at the *miR290* and *Pou5f1* loci (Fig 6A and 6C) were analyzed by quantitative real-time PCR using custom Taqman probes. The amount of DNA in the qPCR reactions was normalized across 3C libraries using a custom Taqman probe directed against the *Actb* locus. Primer and probe sequences are listed in Supplemental Table 5.

QUANTIFICATION AND STATISTICAL ANALYSIS

Statistical parameters including the exact value of n, the definition of center, dispersion and precision measures (mean ± SEM) and statistical significance are reported in the Figures and the Figure Legends. Data is judged to be statistically significant when $p < 0.05$ by two-tailed Student's T-Test or 2-way ANOVA, where appropriate.

DATA AND SOFTWARE AVAILABILITY

Raw data files for the ChIP-seq analysis have been deposited in the NCBI Gene Expression Omnibus under accession number GSE83890.

Supplementary Material

Refer to Web version on PubMed Central for supplementary material.

Acknowledgments

We thank Patti Wisniewski and Colin Zollo for FACS sorting, and thank Chuan He, Michael Greenberg, Robert Weinberg, Yupeng He, Joseph Ecker, Klaus Kaestner, Zipeng Fan, Chikdu Shivalila, Dongdong Fu, Johanna Goldmann, Carrie Garrett-Engele, Malkiel Cohen, Robert Plasschaert, Frank Soldner, and Bluma Lesch for reagents, technical assistance and inputs on the manuscript. This study was supported by NIH grants HD045022 and HG002668. X.S.L. is supported by a Damon Runyon Cancer Foundation Postdoctoral Fellowship, H.W. is supported by a NARSAD Young Investigator Fellowship, X.W. is supported by a Helen Hay Whitney Foundation Postdoctoral Fellowship, S.C. is supported by the HARMONIA grant No. UMO-2014/14/M/NZ1/00010 from the National Science Centre in Poland, and Y.S. is supported by a Human Frontier Science Program postdoctoral fellowship. R.J. is co-founder of Fate Therapeutics and Fulcrum Therapeutics and an adviser to Stemgent and R.A.Y is a founder of Syros Pharmaceuticals.

REFERENCES

Bell AC, Felsenfeld G. Methylation of a CTCF-dependent boundary controls imprinted expression of the Igf2 gene. Nature. 2000; 405:482–485. [PubMed: 10839546]

Bernstein DL, Le Lay JE, Ruano EG, Kaestner KH. TALE-mediated epigenetic suppression of CDKN2A increases replication in human fibroblasts. J Clin Invest. 2015; 125:1998–2006. [PubMed: 25866970]

Bird A. DNA methylation patterns and epigenetic memory. Genes Dev. 2002; 16:6–21. [PubMed: 11782440]

Brunk BP, Goldhamer DJ, Emerson CP Jr. Regulated demethylation of the myoD distal enhancer during skeletal myogenesis. Dev Biol. 1996; 177:490–503. [PubMed: 8806826]

Chen B, Gilbert LA, Cimini BA, Schnitzbauer J, Zhang W, Li GW, Park J, Blackburn EH, Weissman JS, Qi LS, et al. Dynamic imaging of genomic loci in living human cells by an optimized CRISPR/Cas system. Cell. 2013; 155:1479–1491. [PubMed: 24360272]

Chen WG, Chang Q, Lin Y, Meissner A, West AE, Griffith EC, Jaenisch R, Greenberg ME. Derepression of BDNF transcription involves calcium-dependent phosphorylation of MeCP2. Science. 2003; 302:885–889. [PubMed: 14593183]

Choudhury SR, Cui Y, Lubecka K, Stefanska B, Irudayaraj J. CRISPR-dCas9 mediated TET1 targeting for selective DNA demethylation at BRCA1 promoter. Oncotarget. 2016

Cong L, Ran FA, Cox D, Lin SL, Barretto R, Habib N, Hsu PD, Wu XB, Jiang WY, Marraffini LA, et al. Multiplex Genome Engineering Using CRISPR/Cas Systems. Science. 2013; 339:819–823. [PubMed: 23287718]

Constantinides PG, Jones PA, Gevers W. Functional striated muscle cells from non-myoblast precursors following 5-azacytidine treatment. Nature. 1977; 267:364–366. [PubMed: 68440]

Davis RL, Weintraub H, Lassar AB. Expression of a single transfected cDNA converts fibroblasts to myoblasts. Cell. 1987; 51:987–1000. [PubMed: 3690668]

Dawlaty MM, Ganz K, Powell BE, Hu YC, Markoulaki S, Cheng AW, Gao Q, Kim J, Choi SW, Page DC, et al. Tet1 is dispensable for maintaining pluripotency and its loss is compatible with embryonic and postnatal development. Cell Stem Cell. 2011; 9:166–175. [PubMed: 21816367]

De Jager PL, Srivastava G, Lunnon K, Burgess J, Schalkwyk LC, Yu L, Eaton ML, Keenan BT, Ernst J, McCabe C, et al. Alzheimer's disease: early alterations in brain DNA methylation at ANK1, BIN1, RHBDF2 and other loci. Nat Neurosci. 2014; 17:1156–1163. [PubMed: 25129075]

Dekker J, Mirny L. The 3D Genome as Moderator of Chromosomal Communication. Cell. 2016; 164:1110–1121. [PubMed: 26967279]

Dixon JR, Selvaraj S, Yue F, Kim A, Li Y, Shen Y, Hu M, Liu JS, Ren B. Topological domains in mammalian genomes identified by analysis of chromatin interactions. Nature. 2012; 485:376–380. [PubMed: 22495300]

Dobin A, Davis CA, Schlesinger F, Drenkow J, Zaleski C, Jha S, Batut P, Chaisson M, Gingeras TR. STAR: ultrafast universal RNA-seq aligner. Bioinformatics. 2013; 29:15–21. [PubMed: 23104886]

Dowen JM, Fan ZP, Hnisz D, Ren G, Abraham BJ, Zhang LN, Weintraub AS, Schuijers J, Lee TI, Zhao K, et al. Control of cell identity genes occurs in insulated neighborhoods in mammalian chromosomes. Cell. 2014; 159:374–387. [PubMed: 25303531]

Ebert DH, Gabel HW, Robinson ND, Kastan NR, Hu LS, Cohen S, Navarro AJ, Lyst MJ, Ekiert R, Bird AP, et al. Activity-dependent phosphorylation of MeCP2 threonine 308 regulates interaction with NCoR. Nature. 2013; 499:341–345. [PubMed: 23770587]

Gibcus JH, Dekker J. The hierarchy of the 3D genome. Mol Cell. 2013; 49:773–782. [PubMed: 23473598]

Gilbert LA, Larson MH, Morsut L, Liu Z, Brar GA, Torres SE, Stern-Ginossar N, Brandman O, Whitehead EH, Doudna JA, et al. CRISPR-mediated modular RNA-guided regulation of transcription in eukaryotes. Cell. 2013; 154:442–451. [PubMed: 23849981]

Gorkin DU, Leung D, Ren B. The 3D genome in transcriptional regulation and pluripotency. Cell Stem Cell. 2014; 14:762–775. [PubMed: 24905166]

Guo JU, Su Y, Zhong C, Ming GL, Song H. Hydroxylation of 5-methylcytosine by TET1 promotes active DNA demethylation in the adult brain. Cell. 2011; 145:423–434. [PubMed: 21496894]

Hilton IB, D'Ippolito AM, Vockley CM, Thakore PI, Crawford GE, Reddy TE, Gersbach CA. Epigenome editing by a CRISPR-Cas9-based acetyltransferase activates genes from promoters and enhancers. Nat Biotechnol. 2015; 33:510–517. [PubMed: 25849900]

Jaenisch R, Bird A. Epigenetic regulation of gene expression: how the genome integrates intrinsic and environmental signals. Nat Genet. 2003; 33(Suppl):245–254. [PubMed: 12610534]

Ji X, Dadon DB, Powell BE, Fan ZP, Borges-Rivera D, Shachar S, Weintraub AS, Hnisz D, Pegoraro G, Lee TI, et al. 3D Chromosome Regulatory Landscape of Human Pluripotent Cells. Cell Stem Cell. 2016; 18:262–275. [PubMed: 26686465]

Jinek M, Chylinski K, Fonfara I, Hauer M, Doudna JA, Charpentier E. A programmable dual-RNA-guided DNA endonuclease in adaptive bacterial immunity. Science. 2012; 337:816–821. [PubMed: 22745249]

Kagey MH, Newman JJ, Bilodeau S, Zhan Y, Orlando DA, van Berkum NL, Ebmeier CC, Goossens J, Rahl PB, Levine SS, et al. Mediator and cohesin connect gene expression and chromatin architecture. Nature. 2010; 467:430–435. [PubMed: 20720539]

Konermann S, Brigham MD, Trevino AE, Joung J, Abudayyeh OO, Barcena C, Hsu PD, Habib N, Gootenberg JS, Nishimasu H, et al. Genome-scale transcriptional activation by an engineered CRISPR-Cas9 complex. Nature. 2015; 517:583–U332. [PubMed: 25494202]

Landau DA, Clement K, Ziller MJ, Boyle P, Fan J, Gu H, Stevenson K, Sougnez C, Wang L, Li S, et al. Locally disordered methylation forms the basis of intratumor methylome variation in chronic lymphocytic leukemia. Cancer Cell. 2014; 26:813–825. [PubMed: 25490447]

Lassar AB, Paterson BM, Weintraub H. Transfection of a DNA locus that mediates the conversion of 10T1/2 fibroblasts to myoblasts. Cell. 1986; 47:649–656. [PubMed: 2430720]

Lin Y, Bloodgood BL, Hauser JL, Lapan AD, Koon AC, Kim TK, Hu LS, Malik AN, Greenberg ME. Activity-dependent regulation of inhibitory synapse development by Npas4. Nature. 2008; 455:1198–1204. [PubMed: 18815592]

Lister R, Mukamel EA, Nery JR, Urich M, Puddifoot CA, Johnson ND, Lucero J, Huang Y, Dwork AJ, Schultz MD, et al. Global Epigenomic Reconfiguration During Mammalian Brain Development. Science. 2013; 341:629.

Lister R, Pelizzola M, Dowen RH, Hawkins RD, Hon G, Tonti-Filippini J, Nery JR, Lee L, Ye Z, Ngo QM, et al. Human DNA methylomes at base resolution show widespread epigenomic differences. Nature. 2009; 462:315–322. [PubMed: 19829295]

Maeder ML, Angstman JF, Richardson ME, Linder SJ, Cascio VM, Tsai SQ, Ho QH, Sander JD, Reyon D, Bernstein BE, et al. Targeted DNA demethylation and activation of endogenous genes using programmable TALE-TET1 fusion proteins. Nat Biotechnol. 2013; 31:1137–1142. [PubMed: 24108092]

Mali P, Yang L, Esvelt KM, Aach J, Guell M, DiCarlo JE, Norville JE, Church GM. RNA-guided human genome engineering via Cas9. Science. 2013; 339:823–826. [PubMed: 23287722]

Martinowich K, Hattori D, Wu H, Fouse S, He F, Hu Y, Fan G, Sun YE. DNA methylation-related chromatin remodeling in activity-dependent BDNF gene regulation. Science. 2003; 302:890–893. [PubMed: 14593184]

Narendra V, Rocha PP, An D, Raviram R, Skok JA, Mazzoni EO, Reinberg D. CTCF establishes discrete functional chromatin domains at the Hox clusters during differentiation. Science. 2015; 347:1017–1021. [PubMed: 25722416]

Nora EP, Lajoie BR, Schulz EG, Giorgetti L, Okamoto I, Servant N, Piolot T, van Berkum NL, Meisig J, Sedat J, et al. Spatial partitioning of the regulatory landscape of the X-inactivation centre. Nature. 2012; 485:381–385. [PubMed: 22495304]

Phillips-Cremins JE, Sauria ME, Sanyal A, Gerasimova TI, Lajoie BR, Bell JS, Ong CT, Hookway TA, Guo C, Sun Y, et al. Architectural protein subclasses shape 3D organization of genomes during lineage commitment. Cell. 2013; 153:1281–1295. [PubMed: 23706625]

Phillips JE, Corces VG. CTCF: master weaver of the genome. Cell. 2009; 137:1194–1211. [PubMed: 19563753]

Qi LS, Larson MH, Gilbert LA, Doudna JA, Weissman JS, Arkin AP, Lim WA. Repurposing CRISPR as an RNA-guided platform for sequence-specific control of gene expression. Cell. 2013; 152:1173–1183. [PubMed: 23452860]

Robertson KD. DNA methylation and human disease. Nat Rev Genet. 2005; 6:597–610. [PubMed: 16136652]

Schultz MD, He Y, Whitaker JW, Hariharan M, Mukamel EA, Leung D, Rajagopal N, Nery JR, Urich MA, Chen H, et al. Human body epigenome maps reveal noncanonical DNA methylation variation. Nature. 2015; 523:212–216. [PubMed: 26030523]

Smith ZD, Meissner A. DNA methylation: roles in mammalian development. Nat Rev Genet. 2013; 14:204–220. [PubMed: 23400093]

Stelzer Y, Shivalila CS, Soldner F, Markoulaki S, Jaenisch R. Tracing dynamic changes of DNA methylation at single-cell resolution. Cell. 2015; 163:218–229. [PubMed: 26406378]

Stelzer Y, Wu H, Song Y, Shivalila CS, Marloulaki S, Jaenisch R. Parent-of-origin DNA methylation dynamics during mouse development. Cell Reports. 2016 in press.

Sweatt JD. The emerging field of neuroepigenetics. Neuron. 2013; 80:624–632. [PubMed: 24183015]

Vojta A, Dobrinic P, Tadic V, Bockor L, Korac P, Julg B, Klasic M, Zoldos V. Repurposing the CRISPR-Cas9 system for targeted DNA methylation. Nucleic Acids Res. 2016; 44:5615–5628. [PubMed: 26969735]

Wang H, Maurano MT, Qu H, Varley KE, Gertz J, Pauli F, Lee K, Canfield T, Weaver M, Sandstrom R, et al. Widespread plasticity in CTCF occupancy linked to DNA methylation. Genome Res. 2012; 22:1680–1688. [PubMed: 22955980]

Wilson MH, Coates CJ, George AL Jr. PiggyBac transposon-mediated gene transfer in human cells. Mol Ther. 2007; 15:139–145. [PubMed: 17164785]

Wu H, Luo J, Yu H, Rattner A, Mo A, Wang Y, Smallwood PM, Erlanger B, Wheelan SJ, Nathans J. Cellular resolution maps of X chromosome inactivation: implications for neural development, function, and disease. Neuron. 2014a; 81:103–119. [PubMed: 24411735]

Wu H, Zhang Y. Reversing DNA methylation: mechanisms, genomics, and biological functions. Cell. 2014; 156:45–68. [PubMed: 24439369]

Wu X, Scott DA, Kriz AJ, Chiu AC, Hsu PD, Dadon DB, Cheng AW, Trevino AE, Konermann S, Chen S, et al. Genome-wide binding of the CRISPR endonuclease Cas9 in mammalian cells. Nat Biotechnol. 2014b; 32:670–676. [PubMed: 24752079]

Xu W, Yang H, Liu Y, Yang Y, Wang P, Kim SH, Ito S, Yang C, Wang P, Xiao MT, et al. Oncometabolite 2-hydroxyglutarate is a competitive inhibitor of alpha-ketoglutarate-dependent dioxygenases. Cancer Cell. 2011; 19:17–30. [PubMed: 21251613]

Xu X, Tao Y, Gao X, Zhang L, Li X, Zou W, Ruan K, Wang F, Xu GL, Hu R. A CRISPR-based approach for targeted DNA demethylation. Cell discovery. 2016; 2:16009. [PubMed: 27462456]

Yu M, Hon GC, Szulwach KE, Song CX, Zhang L, Kim A, Li X, Dai Q, Shen Y, Park B, et al. Base-resolution analysis of 5-hydroxymethylcytosine in the mammalian genome. Cell. 2012; 149:1368–1380. [PubMed: 22608086]

Zhang Y, Liu T, Meyer CA, Eeckhoute J, Johnson DS, Bernstein BE, Nusbaum C, Myers RM, Brown M, Li W, et al. Model-based analysis of ChIP-Seq (MACS). Genome Biol. 2008; 9:R137. [PubMed: 18798982]

highlights

- dCas9-Tet1 and -Dnmt3a enable precise editing of CpG methylation *in vitro* and *in vivo*
- Targeted demethylation of *BDNF* promoter IV activates BDNF in neurons
- Targeted enhancer demethylation facilitates MyoD-induced muscle cell reprogramming
- Targeted *de novo* methylation of CTCF motifs alters CTCF-mediated chromatin loops

In brief

DNA methylation patterns can be specifically altered in mammalian cells using CRISPR/Cas9-based approaches.

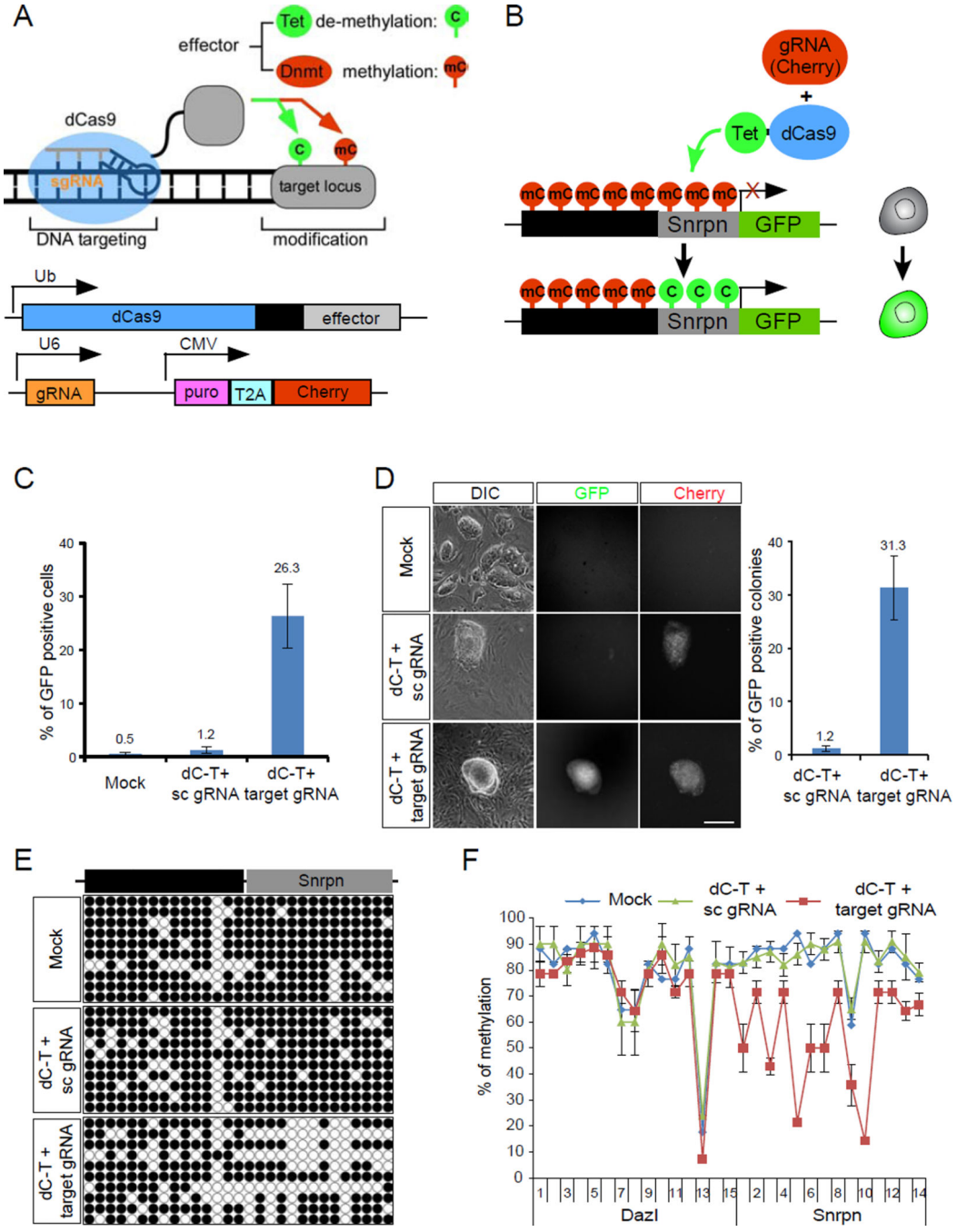

Figure 1.

Activation of the Dazl-Snrpn-GFP reporter by dCas9-Tet1.

(A) Upper panel: schematic representation of a catalytic inactive mutant Cas9 (dCas9) fused with Tet1 for erasing DNA methylation, and with Dnmt3a for *de novo* methylation of specific sequences. Lower panel: an optimized dCas9-effector construct and a guide RNA construct with *puro* and *Cherry* cassettes.

(B) Schematic representation of targeting the *Snrpn* promoter region by dCas9-Tet1 with specific gRNAs to erase methylation and activate GFP expression.

(C) Dazl-Snrpn-GFP mESCs were infected with lentiviruses expressing dCas9-Tet1 (dC-T) with a scrambled gRNA (sc gRNA) or 4 gRNAs targeting the *Snrpn* promoter region (target gRNA). Percentage of GFP positive cells were calculated by flow cytometric analysis of these cells 3-day post infection, and shown as the mean percentages of GFP positive cells ± SD of two biological replicates. Note that the percentages of GFP-positive cells are expressed as the fraction of infected Cherry-positive cells.

(D) Left, representative fluorescence images of the sorted Cherry positive cells in C after culturing for 1 week. Scale bar: 250 um. Right, percentages of GFP positive colonies were quantified, and shown as the mean percentages of GFP positive cells ± SD of two biological replicates.

(E) Bisulfite sequencing of cells described in C.

(F) Methylation levels of individual CpGs in the *Snrpn* promoter region and the adjacent *Dazl* locus. Shown is the mean percentage ± SD of two biological replicates. See also Figure S1 and S2.

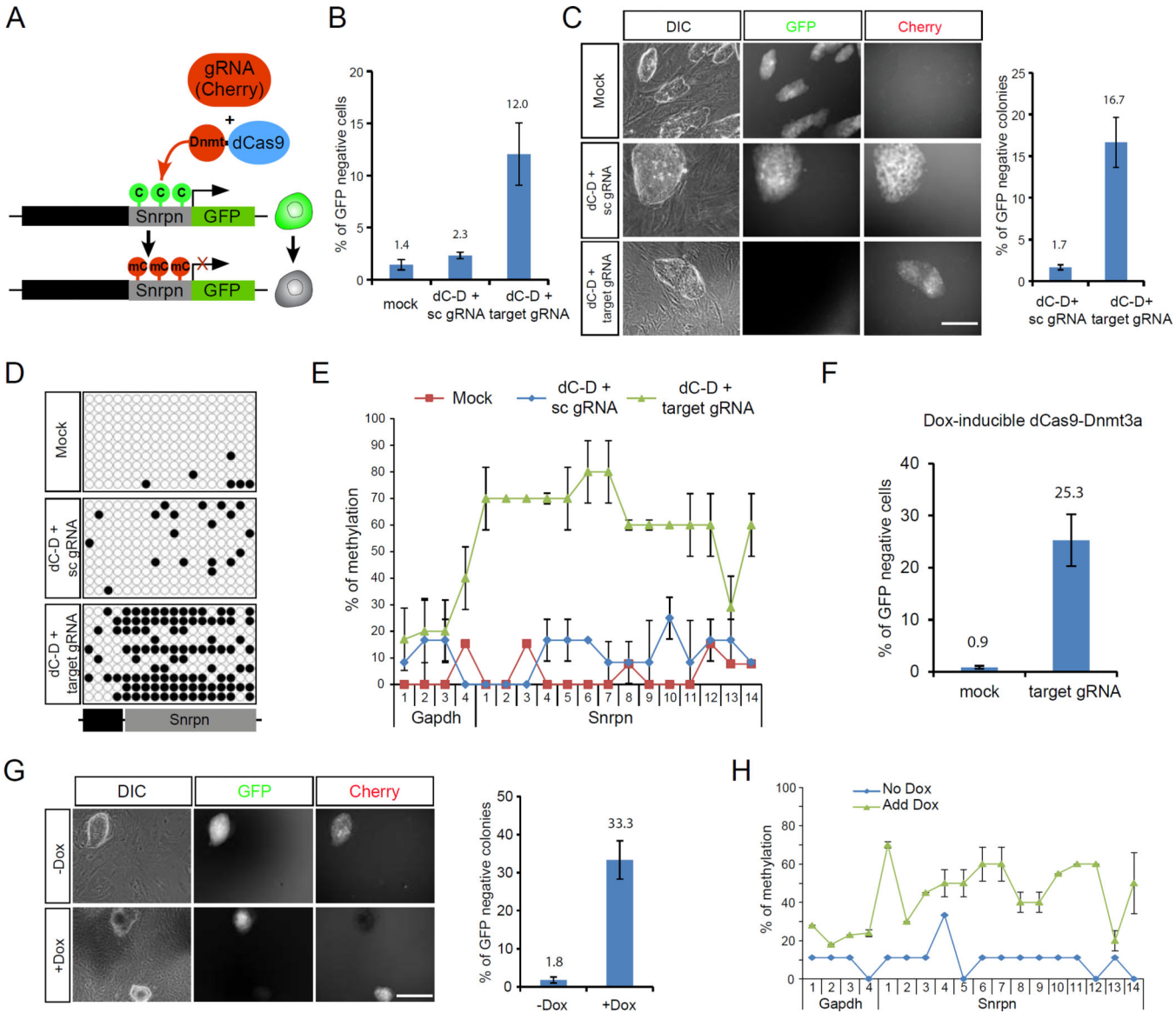

Figure 2.

Silencing of the Gapdh-Snrpn-GFP reporter by dCas9-Dnmt3a.

(A) Schematic representation of targeting the *Snrpn* promoter region by dCas9-Dnmt3a with specific gRNAs to methylate the promoter and silence GFP expression.

(B) Gapdh-Snrpn-GFP mESCs were infected with lentiviruses expressing dCas9-Dnmt3a (dC-D) with a scrambled gRNA (sc gRNA) or gRNAs targeting the *Snrpn* promoter region (target gRNA). Percentage of GFP negative cells was calculated by flow cytometric analysis 3-days after infection, and is shown as the mean percentages of GFP negative cells ± SD of two biological replicates. Note that the percentages of GFP-positive cells are expressed as the fraction of infected Cherry-positive cells.

(C) Left, representative fluorescence images of the sorted Cherry-positive cells in B after culturing for 1 week. Scale bar: 250 um. Right, percentages of GFP negative colonies were

quantified, and are shown as the mean percentages of GFP negative cells ± SD of two biological replicates.

(D) Bisulfite sequencing of cells described in B.

(E) Methylation levels of individual CpGs in the *Snrpn* promoter region and the adjacent *Gapdh* locus. Shown is the mean percentage ± SD of two biological replicates.

(F) Gapdh-Snrpn-GFP mESCs with Doxycycline-inducible dCas9-Dnmt3a were infected with lentiviruses expressing gRNAs targeting the *Snrpn* promoter region in the presence of Doxycycline (2 ug/ml). Percentages of GFP negative cells were calculated by flow cytometric analysis 3-day after infection, and are shown as the mean percentages of GFP negative cells ± SD of two biological replicates. Note that the percentages of GFP-positive cells are expressed as the fraction of infected Cherry-positive cells.

(G) Left, representative fluorescence images of the sorted Cherry-positive population in F after culturing for 1 week with or without Doxycycline. Scale bar: 250 um. Right, percentages of GFP negative colonies were quantified, and are shown as the mean percentages of GFP negative cells ± SD of two biological replicates.

(H) Methylation level of each individual CpG in the *Snrpn* promoter region and the adjacent *Gapdh* locus from cells in G. Shown is the mean percentage ± SD of two biological replicates. See also Figure S2.

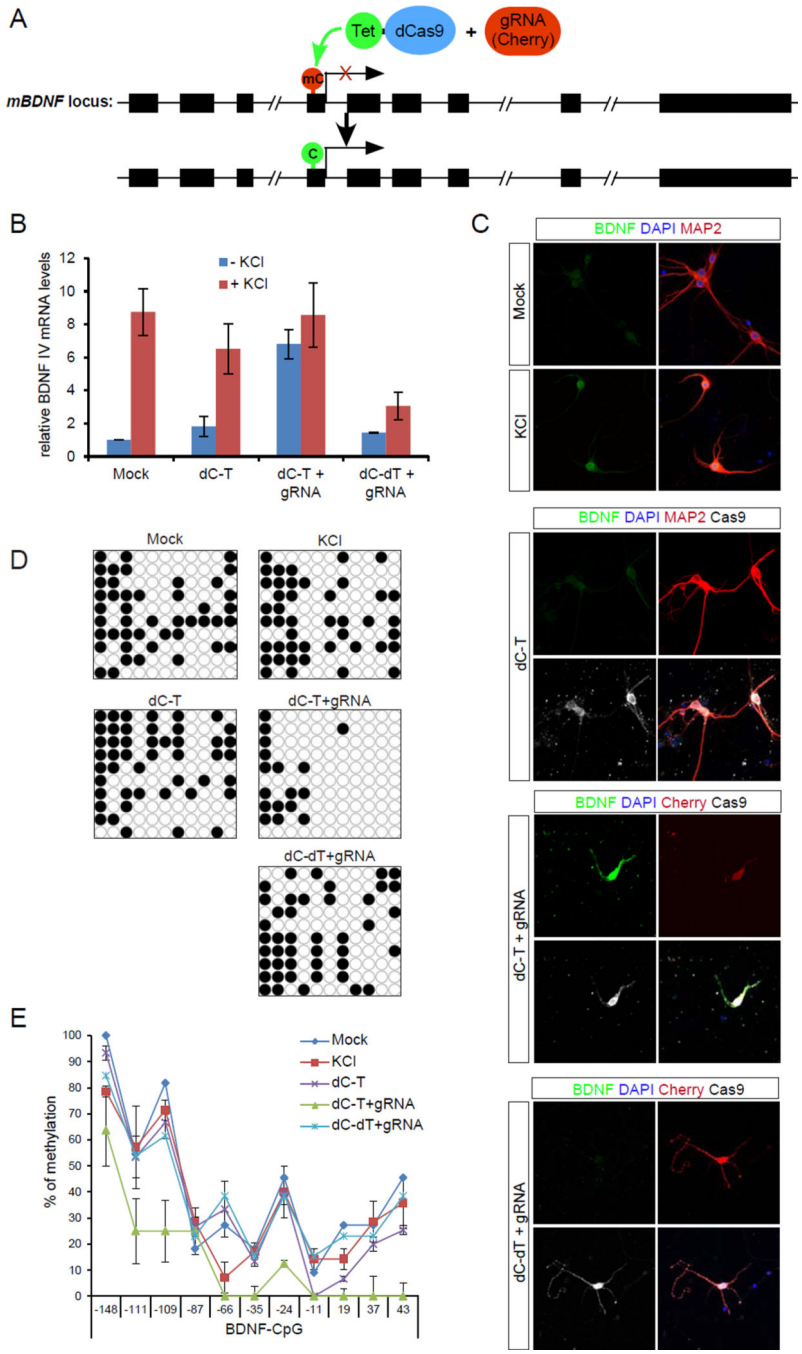

Figure 3.

Targeted demethylation of *BDNF* promoter IV by dCas9-Tet1 to activate BDNF in neurons.

(A) Schematic representation of targeting *BDNF* promoter IV by dCas9-Tet1 (dC-T) with specific gRNAs to erase methylation and activate BDNF expression.

(B) Mouse cortical neurons cultured *in vitro* for 3 days (DIV3) were infected with lentiviruses expressing dC-T with or without gRNAs targeting the *BDNF* promoter IV, or a catalytic dead form of Tet1 (dC-dT) with *BDNF* gRNAs for 2 days, and then treated with or

without KCl (50 mM) for 6 hours before harvesting for RT-qPCR analysis. Bars are mean ± SD of three biological replicates.

(C) Representative confocal images for BDNF induction in B. Stained in red for MAP2 (top two panels) or Cherry (bottom two panels), green for BDNF, blue for DAPI and grey for dCas9. Scale bar: 50 um.

(D) Bisulfite sequencing of neurons in C.

(E) Methylation levels of each individual CpGs in the *BDNF* promoter IV region. Shown is the mean percentage ± SD of two biological replicates.

See also Figure S4.

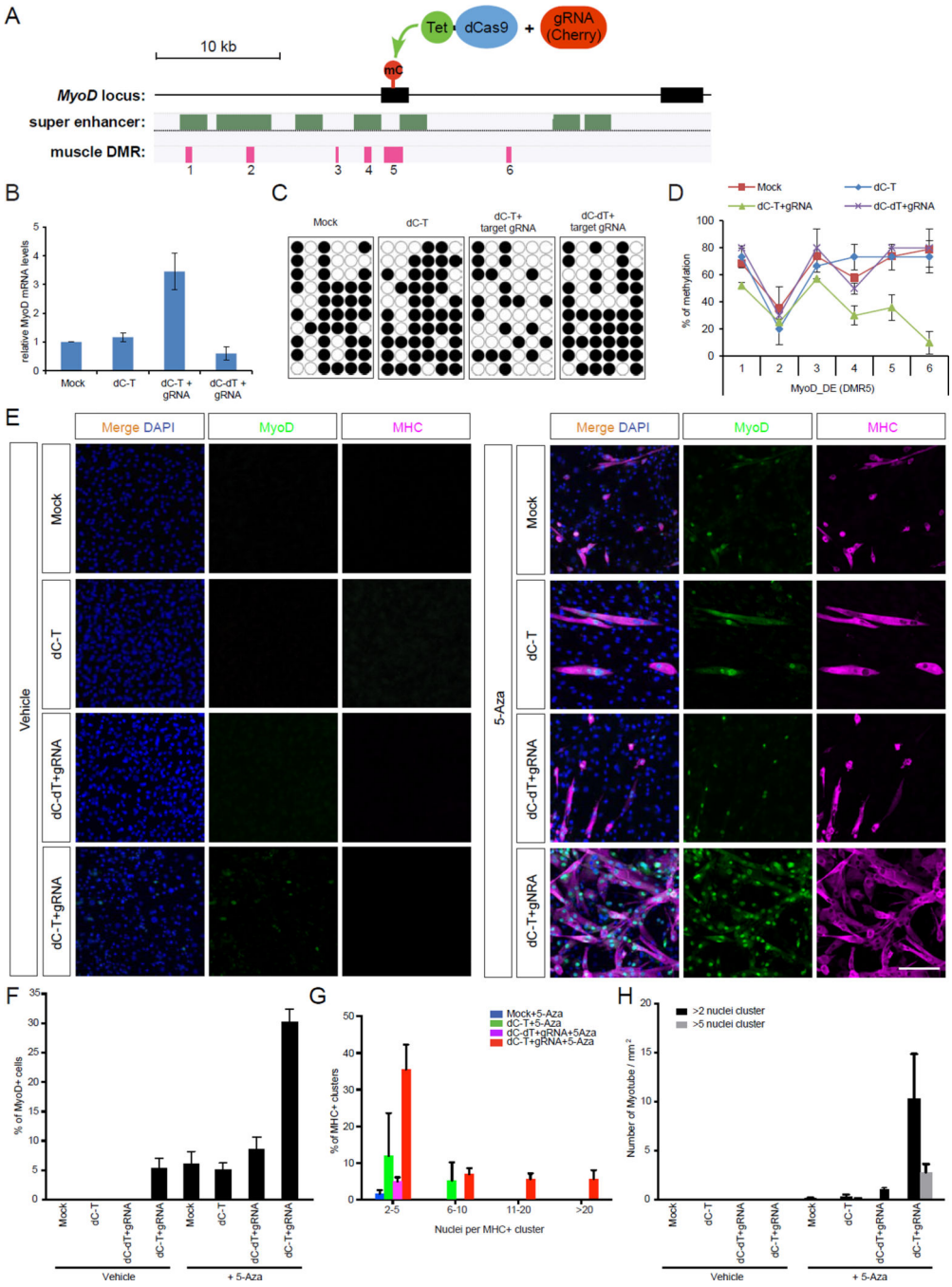

Figure 4.

Targeted demethylation of the *MyoD* distal enhancer by dCas9-Tet1 to facilitate conversion of fibroblasts to myoblasts.

(A) Schematic representation of targeting the *MyoD* distal enhancer (DE) region in DMR-5 by dCas9-Tet1 (dC-T) with specific gRNAs.

(B) C3H10T1/2 cells were infected with lentiviruses expressing dC-T with target gRNAs, or a catalytic dead form of Tet1 (dC-dT) with target gRNAs for 2 days. Cherry positive cells

were FACS sorted for RT-qPCR analysis. Bars represent mean ± SD of three experimental replicates.

(C) Bisulfite sequencing of cells in B.

(D) Methylation level of individual CpGs in the *MyoD* DE region. Shown is the mean percentage ± SD of two biological replicates.

(E) Representative confocal images for C3H10T1/2 cells on day 14 in the fibroblast-to-myoblast conversion assay. Stained in green for MyoD, magenta for MHC and blue for DAPI. Scale bar: 200 um.

(F) Quantification of MyoD positive cell ratio 14-day post infection with lentiviruses expressing dC-T alone, dC-T or dC-dT with gRNAs targeting DMR-5.

(G) Distribution profile of MHC positive cell clusters based on nuclei number per MHC+ cluster (grouped as 2–5, 6–10, 11–20 and >20 nuclei per MHC+ cluster) 14-days post infection.

(H) Quantification of myotube density in MHC positive clusters with more than 2 or 5 nuclei at 14-days after infection. Data are quantified from 3–5 representative images for F-H. Bars represent mean ± SD.

See also Figure S5.

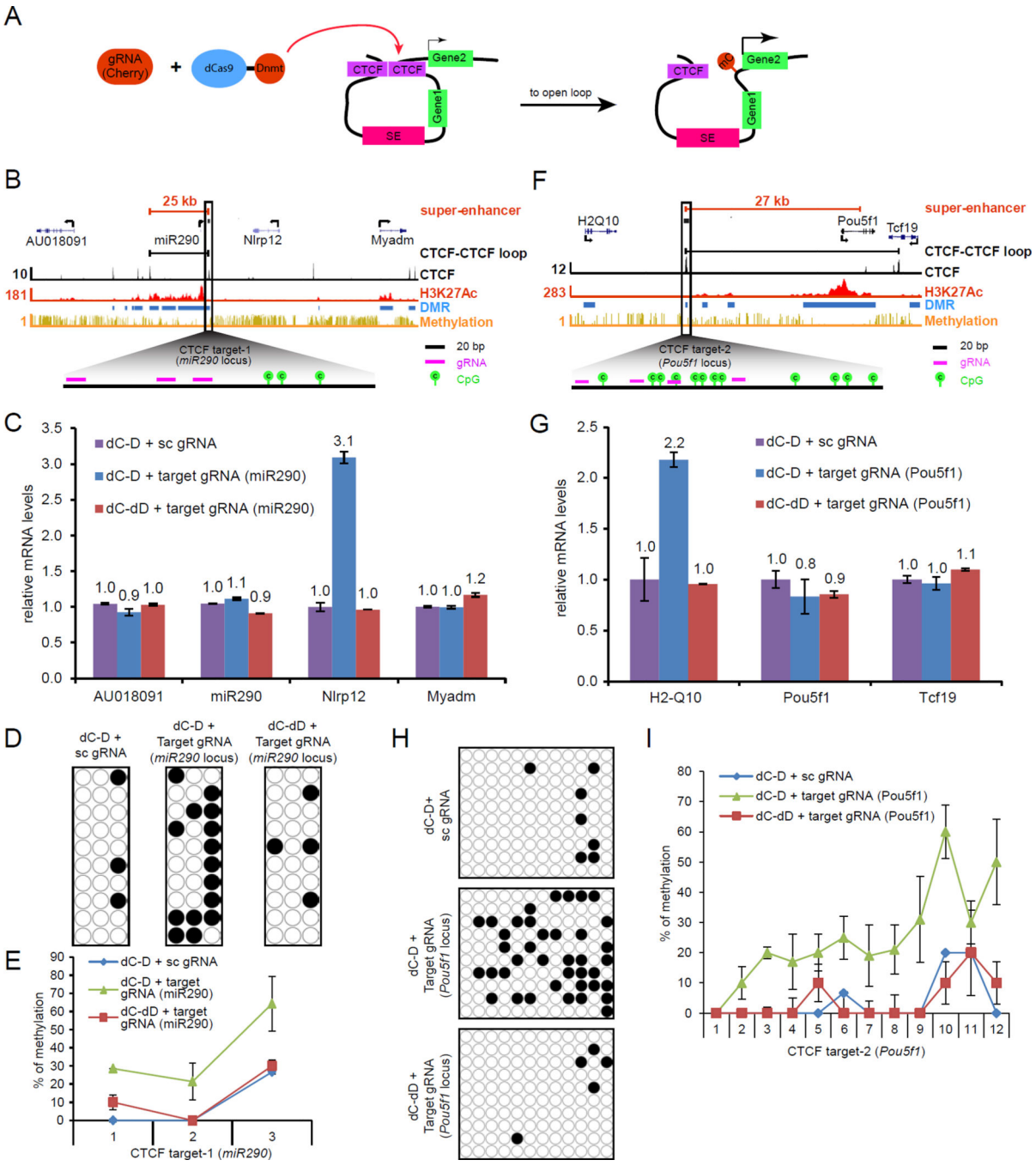

Figure 5.

Targeted methylation of CTCF binding sites.

(A) Schematic representation of targeting the CTCF binding site by dCas9-Dnmt3a with specific gRNAs to induce *de novo* methylation, blocking CTCF recruitment, and opening CTCF loops which alters gene expression in the adjacent loop.

(B) Schematic representation of CTCF target-1 (*miR290* locus) with super-enhancer and *miR290* in the loop, *AU018091* gene in the left neighboring loop, and *Nlrp12* gene in the right neighboring loop (close to the targeted CTCF binding site). The *Myadm* gene is in the

adjacent loop right to the loop containing *Nlrp12*. The super-enhancer domain is indicated as a red bar. The targeted CTCF site is highlighted with a box. ChIP-seq binding profiles (reads per million per base pair) for CTCF in black and H3K27Ac (super-enhancer) in red, and methylation track in yellow with DMR in blue are also shown.

(C–E) Doxycycline-inducible dCas9-Dnmt3a mESCs were infected with lentiviruses expressing a scrambled gRNA or CTCF target-1 gRNAs. Cherry-positive cells were FACS sorted, cultured in the presence of Doxycycline, and then harvested for RT-qPCR analysis in C, for bisulfite-sequencing analysis in D&E. Bars represent mean ± SD of three experimental replicates.

(F) Schematic representation of CTCF target-2 with super-enhancer and Pou5f1 gene in this loop as in B.

(G–I) The same set of experiments were performed as described in C-E for CTCF target-2, and cells were harvested for RT-qPCR analysis as in C and for bisulfite sequencing as in D and E. Bars represent mean ± SD of three experimental replicates.

See also Figure S6.

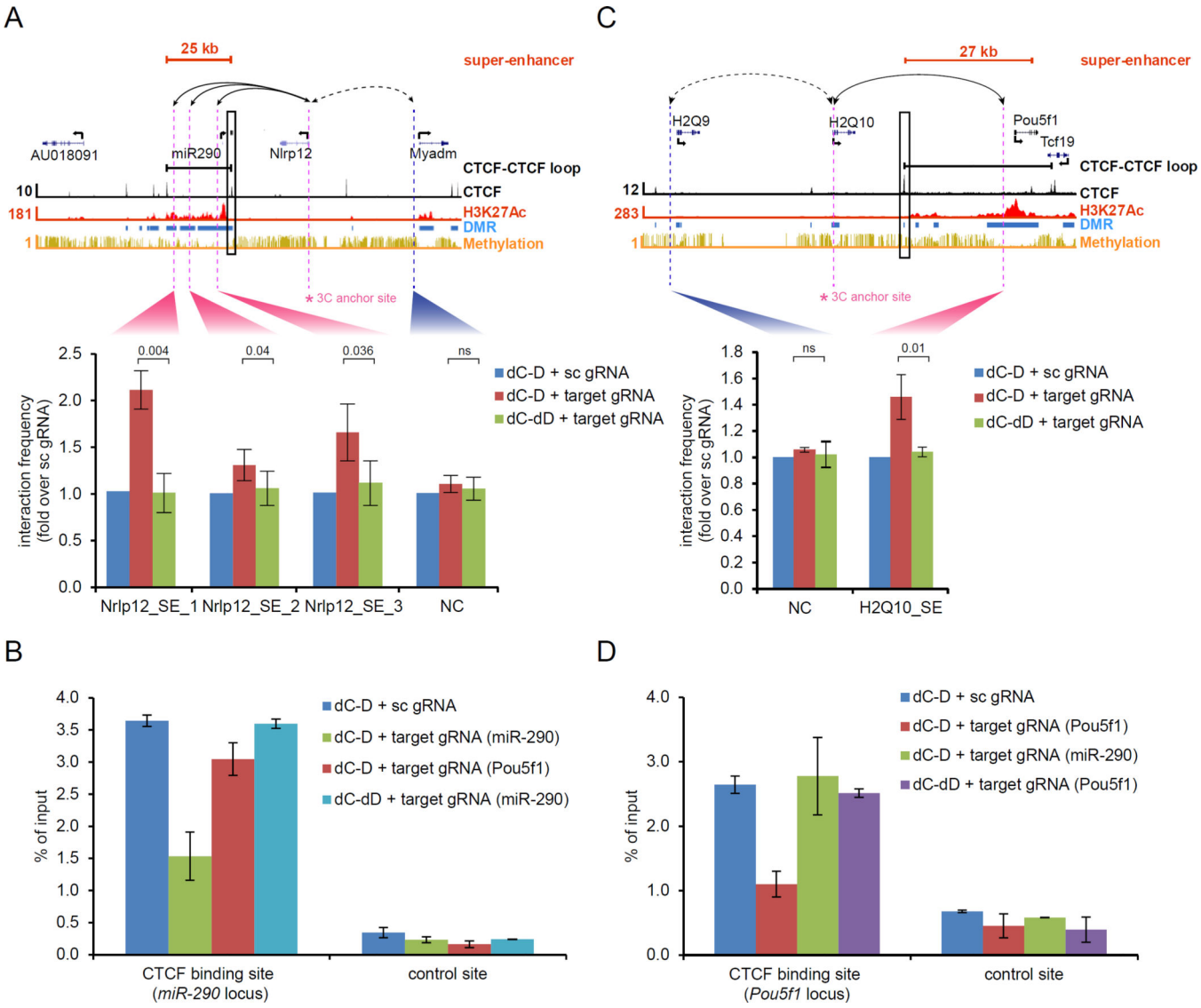

Figure 6.

Targeted methylation of CTCF binding sites to manipulate CTCF loops.

(A) Quantitative Chromosome Conformation Capture (3C) analysis of cells described in Fig 5C at the *miR290* locus. The super-enhancer domain is indicated as a red bar. The targeted CTCF site is highlighted with a box. Arrows indicate the chromosomal positions between which the interaction frequency was assayed. Asterisk indicates the 3C anchor site. ChIP-seq binding profiles (reads per million base pair) for CTCF in black and H3K27Ac (super-enhancer) in red, and methylation track in yellow with DMR in blue are also shown. The interaction frequencies between the indicated chromosomal positions and the 3C anchor sites are displayed as a bar chart (mean ± SD) on the bottom panel. qPCR reactions were run in duplicates, and values are normalized against the mean interaction frequency in cells with a scrambled gRNA. ($p < 0.05$ for all three regions; Student's t test, ns stands for non-significant, NC stands for negative control.)

(B) Anti-CTCF ChIP experiment was performed using cells in A followed by quantitative PCR analysis. Bars represent mean ± SD of three experimental replicates.
(C) Quantitative Chromosome Conformation Capture (3C) analysis of cells described in Fig 5G at the *Pou5f1* locus as in A.
(D) Anti-CTCF ChIP experiment was performed using cells in C followed by quantitative PCR analysis. Bars represent mean ± SD of three experimental replicates.

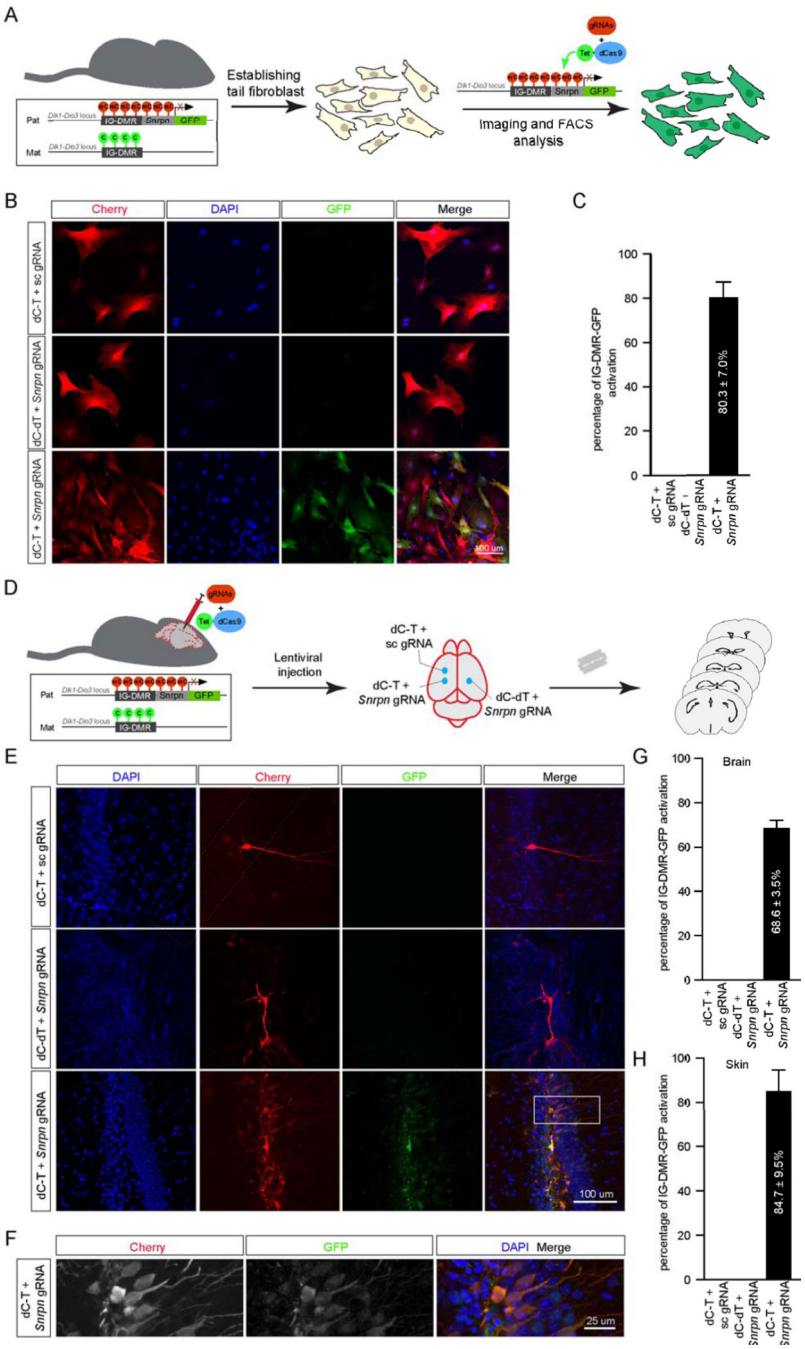

Figure 7.

Targeted *ex vivo* and *in vivo* DNA methylation editing by dCas9-Tet1 to activate a silenced GFP reporter.

(A) Schematic diagram illustrating the experimental procedure for the *ex vivo* activation of a silenced GFP reporter in mouse fibroblast cells. Mouse tail fibroblast cells were derived from a genetically modified mouse line carrying a paternal IG-DMR-Snrpn-GFP allele (IG-DMR$^{GFP/Pat}$) in the *Dlk1-Dio3* locus. The *IG-DMR-Snrpn* promoter on the paternal allele is hypermethylated so that the GFP reporter is constitutively silenced. The cultured fibroblast

cells were infected with lentiviral vectors expressing dCas9-Tet1 and gRNAs to demethylate the *Snrpn* promoter and activate the GFP reporter.

(B) Representative immunohistochemical images of IG-DMR$^{GFP/Pat}$ fibroblasts infected with lentiviruses expressing dCas9-Tet1 (dC-T) with a sc gRNA, an inactive form of dCas9-Tet1 (dC-dT) with *Snrpn* target gRNA, or dCas9-Tet1 with *Snrpn* target gRNA. Stained in red for Cherry, green for GFP and DAPI for nuclei. Scale bar: 100 um.

(C) Quantification of the percentage of IG-DMR$^{GFP/Pat}$ mouse fibroblast cells with GFP activation in Cherry (gRNAs) positive cells. Bars represent mean ± SD of three experimental replicates.

(D) Schematic diagram illustrating the experimental procedure for *in vivo* activation of GFP reporter in the IG-DMR$^{GFP/Pat}$ mouse brain. Lentiviral vectors expressing dC-T and sc gRNA, dC-dT and *Snrpn* target gRNAs, and dC-T and *Snrpn* target gRNAs were delivered with stereotaxic microinjection approach. Brains were sliced and analyzed by immunohistochemical approaches.

(E) Representative confocal micrographs for the IG-DMR$^{GFP/Pat}$ mouse brains infected with dC-T and sc gRNA, dC-dT and *Snrpn* target gRNAs, and dC-T and *Snrpn* target gRNAs. Only dC-T with the target gRNAs activated the GFP expression. Scale bar: 100 um.

(F) Confocal micrograph of the boxed area in E. Stained in red for Cherry, green for GFP and DAPI for nuclei in E and F. Scale bar: 25 um.

(G–H) Quantification of the percentage of IG-DMR$^{GFP/Pat}$ cells with GFP activation in Cherry (gRNAs) positive cells in the *in vivo* lentiviral delivery experiment in the brain (G) and in the skin epidemis (H). Bars represent mean ± SD of more than four representative images from 2 animals.

See also Figure S7.

KEY RESOURCES TABLE

REAGENT or RESOURCE	SOURCE	IDENTIFIER
Antibodies		
Mouse monoclonal anti-Cas9 (IF staining)	Active Motif	Cat#61577 (7A9-3A3)
Mouse monoclonal anti-Cas9 (ChIP)	Active Motif	Cat#61757 (8C1-F10)
Rabbit polyclonal anti-CTCF	EMD Millipore	Cat#07729
Chicken polyclonal anti-GFP	Aves Labs	Cat#GFP-1020
Rabbit polyclonal anti-BDNF	Thermo Fisher SCIENTIFIC	Cat#OSB00017W
Chicken polyclonal anti-MAP2	Encor Biotech	Cat# CPCA-MAP2
Mouse monoclonal anti-MAP2	Sigma-Aldrich	Cat#M2320
Mouse monoclonal anti-Tuj1	Biolegend	Cat#MMS-435P
Rabbit polyclonal anti-MyoD (C-20)	Santa Cruz Biotechnology	Cat#sc-304
Mouse monoclonal anti-MHC (MF20)	R&D systems	Cat#MAB4470
Mouse monoclonal anti-MyoG (F5G)	Thermo Fisher SCIENTIFIC	Cat#MA5-11486
Chemicals		
2-Hydroxyglutarate	TRC Toronto Research Chemicals	Cat#H942596
ABT-888	Selleck	Cat#S1004
5-Aza-2’-deoxycytidine	Sigma Aldrich	Cat#A3656-5MG
Doxycycline hyclate	Sigma Aldrich	Cat#D9891-100G
Critical Commercial Assays		
EpiTect Bisulfite Kit	Qiagen	Cat#59104
TAB-seq kit	Wisegene	Cat#K001
DNeasy Blood & Tissue Kit	Qiagen	Cat#69504
Zymoclean Gel DNA Recovery Kit	Zymo Research	Cat#D4002
DNA Clean & Concentrator-5	Zymo Research	Cat#D4013
X-tremeGENE™ 9 DNA Transfection Reagent	Sigma Aldrich	Cat#6365809001
Xfect™ mESC Transfection Reagent	Clontech	Cat#631320
Direct-zol RNA Miniprep	Zymo Research	Cat#R2050
SuperScript III First-Strand Synthesis SuperMix	Life Technologies	Cat#18080400
Fast SYBR Green Master Mix	Life Technologies	Cat#4385618
Papain neural tissue dissociation system	Worthington Biochemicals	Cat#LK003150
Deposited Data		
Raw data files for RNA sequencing	NCBI Gene Expression Omnibus	GSE83890
Experimental Models: Organisms/Strains		
Mouse: C57Bl/6J	Jackson Laboratories	RRID:IMSR_JAX:000664
Mouse: B6; Tet1 KO mouse	Dawlaty et al., 2011	N/A
Mouse: B6; Dlk1-Dio3 IG-DMR-Snrpn-GFP	Stelzer et al., 2016 (in press)	N/A
Experimental Models: Cell Lines		
V6.5 mESC (C57BL/6 x 129S4/SvJae)	Brambrink et al., 2006	N/A

REAGENT or RESOURCE	SOURCE	IDENTIFIER
Dazl-Snrpn-GFP V6.5 mESC	Stelzer et al., 2015	N/A
Gapdh-Snrpn-GFP V6.5 mESC	Stelzer et al., 2015	N/A
C3H10T1/2 cell line	Constantinides et al., 1977	N/A
Recombinant DNA		
dCas9-Tet/Dnmt	This paper	N/A
pgRNA	This paper	N/A
See “Plasmid design and construction” in METHOD DETAILS section		
Sequence-Based Reagents		
See Table S2, S3, S4, S4 for primer sequences	This paper	N/A
Software and Algorithms		
MACS (ChIP-seq algorithms)	Wu et al., 2014b	http://liulab.dfci.harvard.edu/MACS/
ImageJ (Fiji)	NIH	http://imagej.net/Fiji